# Part II

# Structure and Dynamics in Block Copolymer Solutions

# Chapter 3

# Heat-induced Self-assembling of Thermosensitive Block Copolymer / SANS Study

## 3.1 Introduction

The microphase separation is governed by the molecular weights, composition, the interaction parameter of the constituent blocks, and polymer concentration if the block copolymer is in a solvent.[1] Two types of transitions, i.e., lattice ordering and order-disorder transition, were reported in a series of works on polystyrene-*block*-polybutadiene (PS-*b*-PB) in a selective solvent.[2–4] The former is a melting of macro-lattice (or disordering of microphase separated structure) to micelles, and the other is dissolution of the micelles. These transitions were found to be thermo- and concentration-reversible, which are due to strong selectivity of the solvent. The solvent used was n-tetradecane (C14), which is a selective solvent for polybutadiene (PB) and a non-solvent for polystyrene (PS). By increasing temperature, PS becomes soluble to C14, which leads to lattice disordering followed by order-disorder transition. Recently, studies on ordering and/or morphological transitions of block copolymers in a selective solvent have been extensively carried out.[5–8] These transitions are ascribed to the temperature and/or concentration dependence of the van der Waals interaction between the polymer chain and solvent.

An amphiphilic block copolymer consisting of hydrophilic and hydrophobic block copolymer chains is expected to undergo micellization in water, where hydrophobic interaction plays a major role in controlling the morphology.[9,10] Aoshima et al. prepared a series of stimuli-responsive block copolymers with polyalcohol branches[11] and

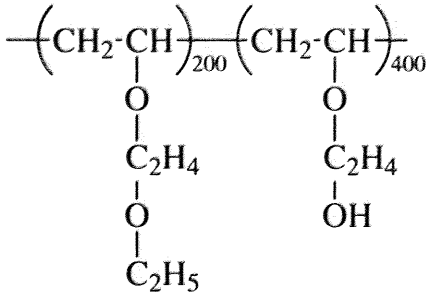

Figure 3.1: Chemical architecture of EOVE-*b*-HOVE.

vinyl ether segments in the side group.[12-14] Because of a narrow molecular weight distribution, a sharp transition in turbidity as well as in viscosity with respect to temperature was observed. Among a variety of combinations, poly(2-ethoxyethyl vinyl ether)-*block*-poly(2-hydroxyethyl vinyl ether) (Figure 3.1; hereafter we abbreviate it as EOVE-*b*-HOVE) aqueous solutions were chosen in this study because they undergo fluidity transition without accompanying serious turbidity. In order to elucidate the origin of this sharp transition, SANS investigation was carried out on a aqueous solutions of EOVE-*b*-HOVE.

## 3.2 Experimental Section

### 3.2.1 Sample

The synthesis of poly(2-ethoxyethyl vinyl ether)-*block*-poly(2-hydroxyethyl vinyl ether), EOVE-*b*-HOVE, involves (i) the preparation of precursor block copolymers by living cationic polymerization of 2-ethoxyethyl vinyl ether (EOVE) and 2-(t-butyldimethylsilyloxy)ethyl vinyl ether (BMSiVE), and (ii) the subsequent conversion of poly(BMSiVE) segments in the precursor block copolymers to polyHOVE segments by acid-promoted hydrolysis.[11] The monomer BMSiVE was prepared by the reaction of 1-(t-butyldimethylsilyl)imidazole with 2-hydroxyethyl vinyl ether (Maruzen Petrochemical) in dimethylformamide at room temperature. The living cationic polymerization was carried out in the presence of ethyl acetate as an added base to stabilize the propagating species.[15] At first, EOVE was polymerized with $CH_3CH(OiBu)OCOCH_3$/-$Et_{1.5}AlCl_{1.5}$ in toluene at 0 °C under a dry nitrogen atmosphere.[16] The second monomer, BMSiVE (neat), was then fed into the polymerization mixture. After a

certain period, the polymerization was quenched with 0.1 wt% ammoniacal methanol. The quenched reaction mixture was diluted with dichloromethane, and then washed with water to remove the initiator residues. The product polymer was recovered from the organic layer by evaporation of the solvents under reduced pressure and vacuum dried overnight. Formation of the desired block copolymers was confirmed by size exclusion chromatography. The composition ratio determined by 1H NMR spectroscopy (JEOL JNM-EX 270) was in agreement with the monomer feed ratio of EOVE and BMSiVE (1/2). Desilylation from EOVE-*b*-BMSiVE was carried out with the addition of 3.0 N aqueous HCl-EtOH to a purified polymer in THF at 0 °C, followed by stirring for 6 h at 0 °C. The mixtures were neutralized, filtered, and isolated by dialysis against Mill-Q water (18 MΩ cm) using a cellulose tube. The EOVE-*b*-HOVE was recovered by evaporation of water under reduced pressure and vacuum dried overnight. Thus, EOVE-*b*-HOVE with $\bar{M}_n = 5.84 \times 10^4$, $\bar{M}_w/\bar{M}_n = 1.07$ was obtained, in which the degrees of polymerizations of EOVE and HOVE are 200 and 400, respectively.

### 3.2.2 Rheological measurement

The dynamic viscoelastic measurement was carried out with a stress-controlled rheometer (Carri-Med CSL2 100, TA-Instruments) with angular frequency of 6:283 rad/s (1Hz). A cone plate with a diameter of 4 cm and an angle of 2 ° was employed. The temperature was controlled within 0.1 °C by a Peltier element.

### 3.2.3 SANS

Since aqueous solutions of EOVE-*b*-HOVE lose fluidity above 20 °C, dry EOVE-*b*-HOVE was dissolved in cold deuterated water at ca. 0 °C and was kept in a refrigerator until use. The concentrations of EOVE-*b*-HOVE were 2, 5, 10, and 17 wt%. The SANS experiment was carried out at the SANS-U. Cold neutrons from the JRR-3M research reactor of Japan Atomic Energy Research Institute, Tokai, Ibaraki, Japan, were monochromatized to a 0.70 nm beam with a neutron velocity selector. The wavelength distribution was 10 %. The sample to detector distance was either 4 or 8 m. The temperature of the sample was regulated with a water circulating bath (NESLAB RTE-111M). Samples in quartz cells of 1 mm or 4 mm thick were irradiated

by the neutron beam for 30 or 60 min depending on the scattering power. The scattered intensity functions were corrected for transmission, and air scattering, and then circularly averaged. The subsequent absolute intensity calibration was carried out with the incoherent scattering from a Lupolen secondary standard sample.[17]

### 3.2.4 Small angle X-ray scattering

Small angle X-ray scattering (SAXS) measurement was carried out on a 17 wt% EOVE-*b*-HOVE aqueous solution at room temperature (ca. 25 °C) with a SAXS instrument (Nano Viewer, Rigaku, Co. Ltd., Japan) equipped with an imaging plate. The X-ray beam was obtained by an X generator (Rigaku Ultrax 18). The operating condition was 45 kV 60 mA and the beam size was $0.3 \times 0.3$ mm$^2$. Monochromatization and intensification was attained with a confocal multi-layered mirror optic (Confocal Max-Flux Optic). A focused Cu K$\alpha$ line (wavelength being 1.54 Å) was used for the SAXS measurement.

### 3.2.5 Differential thermal calorimetry

A high-sensitivity differential scanning calorimeter, DSC8230 (Rigaku, Co. Ltd., Japan), was used to study the endothermic enthalpy. About 26 mg of polymer sample was placed in a stainless pan (resistance to pressure at 50 atm, $3 \times 5$ mm$^{\phi}$ for the vessel size) and then carefully sealed. Thermograms were obtained at rates of 1 °C/min in heating scans between -10 and 80 °C, with water in a stainless pan as a reference.

## 3.3 Results and discussion

### 3.3.1 Rheological transition

Figure 3.2 shows a temperature scan of the storage ($G'$) and loss moduli ($G''$) for a 20 wt% EOVE-*b*-HOVE aqueous solution. This shows a sharp transition in both $G'$ and $G''$ around 20 °C. It is surprising that the change in $G'$ is more than four orders of magnitude and the temperature window of the transition is less than a degree of centigrade. A similar transition was also observed for a 10 wt% EOVE-*b*-HOVE aqueous solution at almost the same temperature.

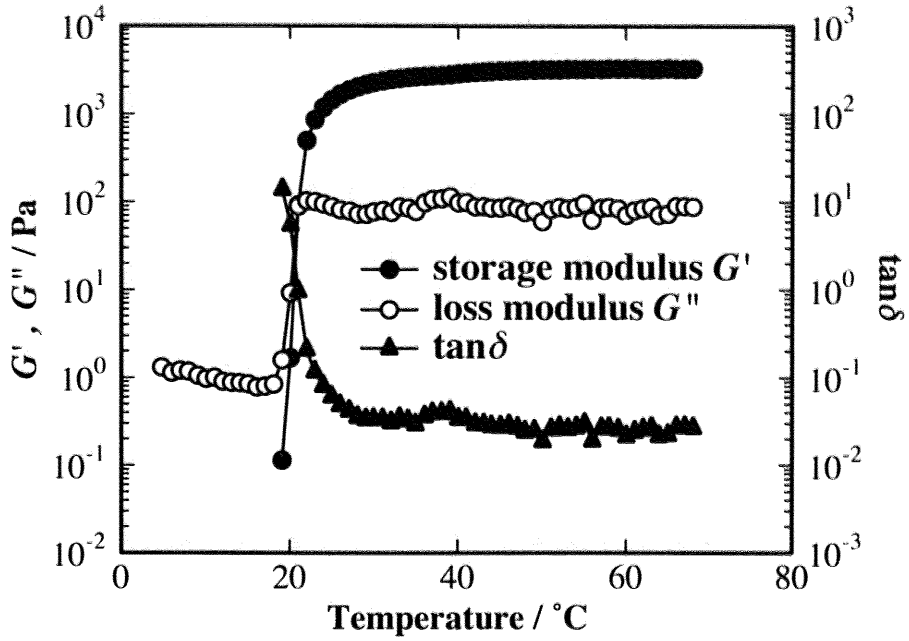


Figure 3.2: Temperature dependence of the storage ($G'$) and loss moduli ($G''$) for EOVE-*b*-HOVE block copolymer aqueous solutions at $w = 20$ wt% (1Hz).

### 3.3.2 SANS analysis

Figure 3.3 shows SANS intensity functions, $I(q)$, of EOVE-*b*-HOVE aqueous solutions at polymer concentrations of (a) $w = 2$, (b) 5, (c) 10, and (d) 17 wt%. Here, $q$ is the momentum transfer. For all concentrations, I(q) was a monotonically decreasing function at low temperatures, i.e., for $T \leq 20$ °C ($w = 2$ wt%), $T \leq 19$ °C ($w = 5$ wt%), $T \leq 17$ °C ($w = 10$ wt%), and $T \leq 16$ °C ($w = 17$ wt%). By increasing temperature, however, the forward scattering increased significantly and scattering peaks appeared. In addition, the peaks shifted toward higher $q$ with increasing $T$. In the case of $w = 17$ wt%, a scattering peak appeared at 17 °C and $I(q)$ grew with further increasing temperature. It should be noted here that additional distinct peaks (denoted by arrows) appear at the lower $q$ region for $T \geq 20$ °C. It is easily deduced that the $I(q)$s with these scattering maxima correspond to the form factor for spherical particles as will be discussed later. In the following, the SANS intensity functions are analyzed in the three regimes, i.e., (i) scattering from polymer solutions, (ii) micelle scattering, and (iii) macrolattice scattering.

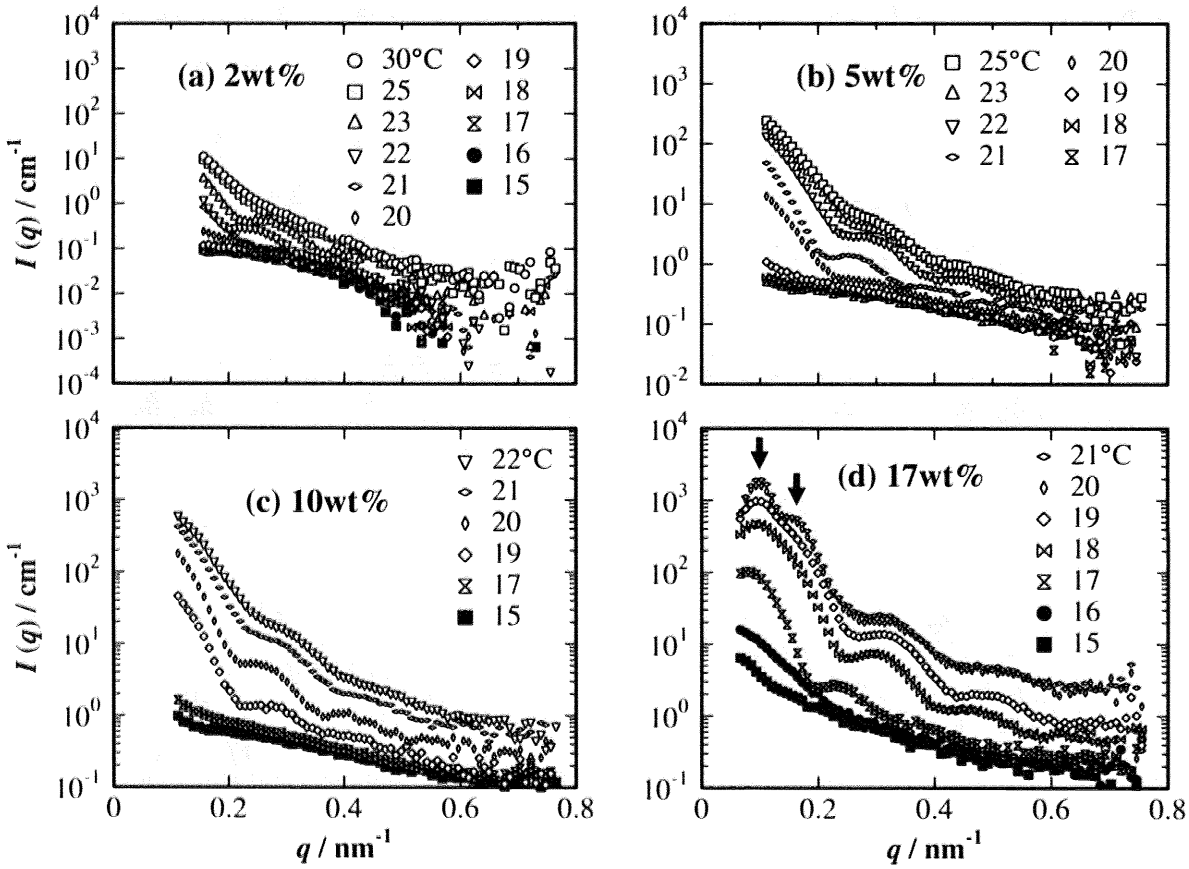


Figure 3.3: SANS scattering intensity curves of EOVE-*b*-HOVE aqueous solutions at (a) $w = 2.0$, (b) 5.0, (c) 10, and (d) 17 wt%. The arrows indicate the interference peaks due to formation of macrolattice.

### Scattering functions from homogeneous polymer solutions

In the semi-dilute regime, the so-called correlation length $\xi$ can be evaluated with the following Ornstein-Zernike equation,

$$I(q) = \frac{I(0)}{1 + \xi^2 q^2} \tag{3.1}$$

The values of the correlation length are about 6.0 nm for 2 wt%, 4.0 nm for 5 and, 3.5 nm for 10 wt% irrespective of $T$. This indicates that $\xi$ is a decreasing function of polymer concentration, $w$. The details will be reported elsewhere.

### Curve fitting with the spherical-particle function

First, let us focus on the particle scattering from spherical domains. The scattering function of spherical particles is given by the following.

$$\Phi(qR) = \frac{3\left[\sin(qR) - qR\cos(qR)\right]}{(qR)^3} \equiv 3\sqrt{\frac{\pi}{2}}\frac{J_{3/2}(qR)}{(qR)^{3/2}} \tag{3.2}$$

where $R$ is the radius of the sphere and $\Phi(x)$ is related to the Bessel Function of the order of 3/2, i.e., $J_{3/2}(x)$. The SANS intensity function for an assembly of dispersed spheres is given by

$$I(q) = nV^2\Delta\rho^2\Phi^2(qR) \tag{3.3}$$

where $n$ is the number of spheres in the unit volume (e.g., $\mathrm{cm}^3$), $V$ is the volume of the sphere, and $\Delta\rho$ is the scattering-length density difference between the sphere and the matrix. The curve fitting of the observed intensity functions was carried out by considering several facts; (1) size distribution of spheres, (2) wavelength distribution of the incident neutron beam, and (3) the instrumental smearing due to a finite size of incident beam.

The size distribution, $W_R(R)$, was assumed to be a Gaussian function given by

$$W_R(R) \sim \exp\left[-\frac{(R - \langle R\rangle)^2}{2\sigma_R^2}\right] \tag{3.4}$$

where $\langle R\rangle$ is the average radius of the sphere. Hence eq. 3.3 has to be rewritten to[18]

$$I_R(q) = \langle n\rangle\Delta\rho^2\frac{\int W(R)V^2(R)\Phi^2(qR)\mathrm{d}R}{\int W(R)\mathrm{d}R} \tag{3.5}$$

Here, $\langle n\rangle$ is the average number of spheres in a unit volume and is given by

$$\langle n\rangle = \frac{w}{d_\mathrm{p}\langle V\rangle} = \frac{\int W(R)\mathrm{d}R}{\int W(R)V\mathrm{d}R} \tag{3.6}$$

The wavelength distribution of the SANS-U is estimated to be FWHM = 10 % around $\langle\lambda\rangle$ = 0.70 nm. Again, a Gaussian distribution was assumed for the wavelength distribution, $W_\lambda(\lambda)$, with

$$W_\lambda(\lambda) \sim \exp\left[-\frac{(\lambda - \langle\lambda\rangle)^2}{2\sigma_\lambda^2}\right], \sigma_\lambda = \frac{\mathrm{FWHM}}{2\sqrt{2\ln 2}} \tag{3.7}$$

and the corrected intensity, $I_{R+\lambda}(q)$, is given in the following form,

$$I_{R+\lambda}(q) = \frac{w}{d_\mathrm{p}}\Delta\rho^2 \frac{\int\int W_R(R)W_\lambda(\lambda)V^2(R)\Phi^2(qR)\mathrm{d}R\mathrm{d}\lambda}{\int\int W_R(R)W_\lambda(\lambda)V(R)\mathrm{d}R\mathrm{d}\lambda} \tag{3.8}$$

The effect of instrumental smearing was also taken into account by convoluting $I(q)$ with the incident beam profile function at the detector plane. The width of the incident beam was evaluated to be $\pm 1.35 \times 10^4$ nm$^{-1}$. It was found that the dominant smearing effect is not due to the wavelength distribution but to the finite size of the incident beam.

Figure 3.4 shows the results of curve fitting for $w$ = 17 wt% at various temperatures. Except for $T$ = 20 and 21 °C, the curve fitting seems to be satisfactory. The same analysis was applied to the other samples having different concentrations.

Figure 3.5 shows the concentration and temperature dependence of (a) the average radius of the core $\langle R\rangle$ and (b) its distribution $\Delta R/\langle R\rangle$. In the case of $w$ = 17 wt%, $\langle R\rangle$ is a decreasing function of $T$, but $\langle R\rangle$ reaches a plateau value of ca. 18.0 nm. Although the values of $\langle R\rangle$ for $w \leq 10$ wt% are somewhat scattered, the values are rather invariant with respect to both temperature for $T \geq 20$ °C and concentration, and are again 18.0 - 20.0 nm. Interestingly, the distribution $\Delta R/\langle R\rangle$ does not change with $w$ or $T$, either. This indicates that the domain size and its distribution are not determined by the environmental variables, such as polymer concentration and temperature (as long as $T \geq 20$ °C), but by the molecular parameters, i.e., the length of polyEOVE and the block composition. It is noteworthy that this is quite different from the case of polystyrene-*block*-polybutadiene in a selective solvent, where the domain size is a strong function of polymer concentration and temperature due to partial solvation by the selective solvent.[3] However, in the case of EOVE-*b*-HOVE, the hydrophobicity of polyEOVE is very strong above 20 °C, resulting in strong exclusion of water from the polyEOVE domain and formation of a spherical domain with a rather unique size. It should also be noted here that the domain size $\langle R\rangle$ is considerably larger than the radius of gyration of the polymer chain, $R_{\mathrm{g},z}$. This means

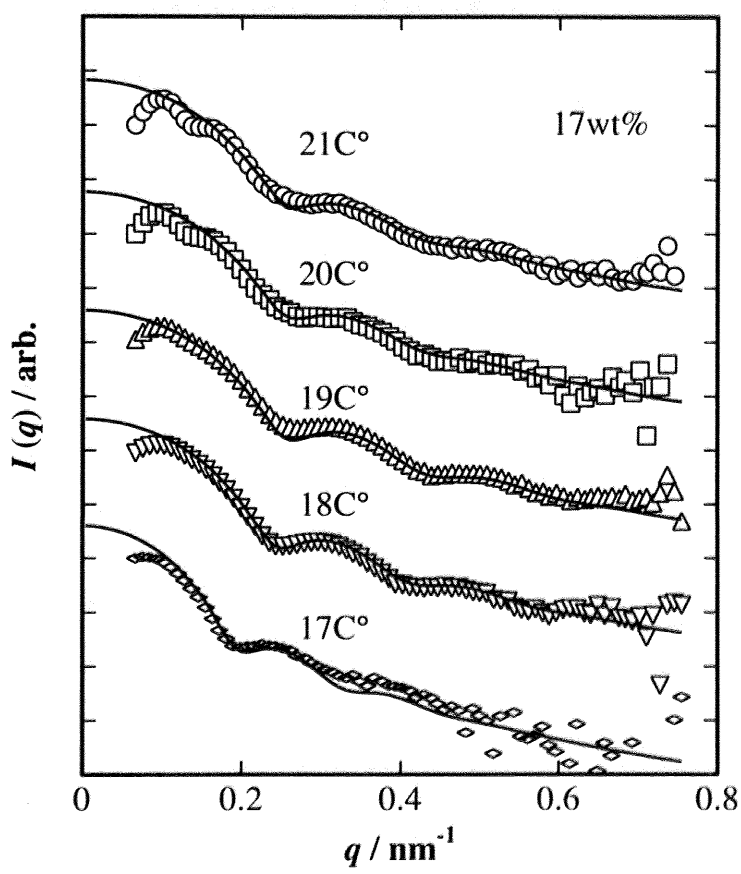


Figure 3.4: Results of curve fit of the SANS scattering intensity functions with eq. 3.8 for EOVE-*b*-HOVE at $w = 17$ wt%.

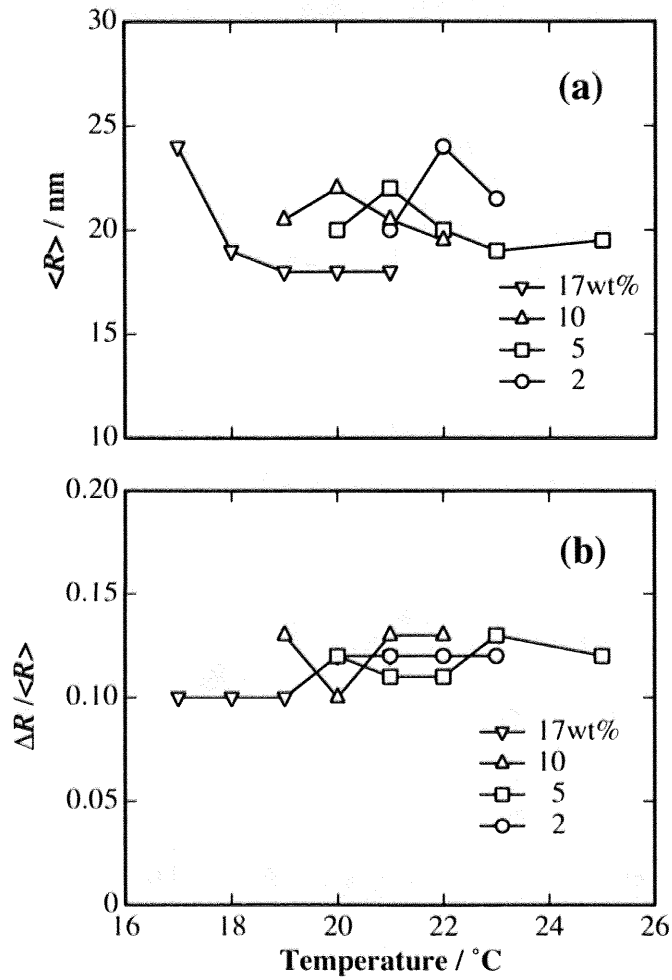


Figure 3.5: Temperature dependence of (a) the average radius of the EOVE domains, $R$, and its distribution, $\Delta R/R$, for EOVE-*b*-HOVE aqueous solutions at various concentrations.

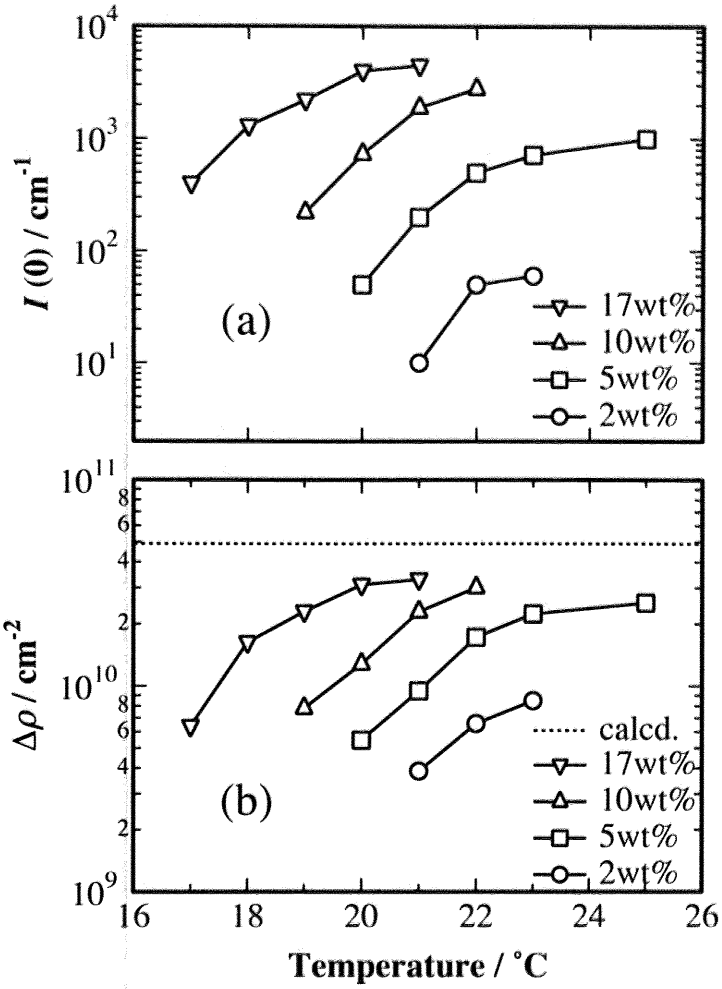


Figure 3.6: Temperature dependence of (a) the zero-$q$ intensity, $I(q = 0)$, and (b) the scattering-length density, $\Delta\rho$. The dashed line indicates the calculated value for the perfect separation of polyEOVE from a mixture of polyHOVE and $D_2O$.

that the polyEOVE chains in the spherical domains are not in the unperturbed but are highly stretched in the radial direction. The driving force of this chain stretching may be the lowering tendency of the total surface area by increasing the radius due to the strong hydrophobic interaction between polyEOVE and the solvent.

Figure 3.6a shows $I(0)$ vs. $T$ for EOVE-$b$-HOVE at various $w$'s. $I(0)$ increases with $T$. This indicates that the micelle formation proceeds and the difference in the scattering length density increases with increasing $T$. Regarding $w$ dependence, $I(0)$ can be normalized with concentration and the volume of the sphere, i.e., $wV$, since $w$ is proportional to $\langle n \rangle$. Note that the number density of the spherical domains remains unchanged irrespective of temperature. By normalizing $I(0)$ with $wV$, one obtains the

variation of the contrast factor, i.e., the scattering-length density difference between the sphere and the matrix, . In Figure 3.6b, $\Delta\rho$ is plotted as a function of $T$, which increases with $T$. The dashed line indicates the theoretical value for perfect separation of polyEOVE from a mixture of polyHOVE and $D_2O$ ($\Delta\rho_0 = 4.9 \times 10^{10}$ $cm^{-2}$). Therefore, this plot shows that phase separation between micelle and matrix proceeds with increasing temperature. Figure 3.7 shows a master curve for the $\Delta\rho$ vs $T + \Delta T$. A horizontal shift was necessary to construct the master curve because the transition temperature is concentration dependent. The shift factor $\Delta T$ is shown in the inset of Figure 3.7a. This indicates that the interaction parameter between polyEOVE and water is a function of polyEOVE concentration as well as temperature and the transition temperature for micellization increases rather linearly with $T$. The dependence of polyEOVE concentration is consistent with our preliminary results by using of homopolymers having the similar structure.[16]

The partition coefficient, i.e., the difference in the fraction of the EOVE segments in the core and the matrix, can be estimated via $\Delta\rho$, with the following equation.[19]

$$\Delta\phi_{\mathrm{EOVE}} \equiv \left(\frac{\Delta\rho}{\Delta\rho_0}\right) = 1 - \exp\left(-\frac{\Delta G}{k_{\mathrm{B}}T}\right) \tag{3.9}$$

$$\frac{\Delta G}{k_{\mathrm{B}}T} = -\ln\left[1 - \Delta\phi_{\mathrm{EOVE}}\right] = \frac{\Delta H}{k_{\mathrm{B}}T} - \frac{\Delta S}{k_{\mathrm{B}}} \tag{3.10}$$

where $k_{\mathrm{B}}$ is the Boltzman constant and $\Delta G(\geq 0)$ is the free energy difference to place an EOVE block chain in the domain and in the matrix, and $\Delta H$ and $\Delta S$ are the corresponding enthalpy and entropy, respectively. $\Delta G$ was evaluated by linear regression of eq. 3.10,

$$\frac{\Delta G}{k_{\mathrm{B}}T} = 25.5 - \frac{7.50 \times 10^3}{T},\ T > 294\ \mathrm{K}\ (\mathrm{for}\ w = 2\mathrm{wt}\%) \tag{3.11}$$

and

$$T = T_{w=2\mathrm{wt}\%} + \Delta T,\ \Delta T = 0.29w \tag{3.12}$$

Figure 3.7b shows the plot of $\Delta G/k_{\mathrm{B}}T$ as a function of $1/T$. The enthalpy of partition, $\Delta H$, is negative ($\approx -15.0$ kcal/mol) and is quite large, resulting in the strong temperature dependence of the phase behavior. The negative sign means that the system has a lower critical solution temperature (LCST), above which a phase separation takes place. The concentration dependence of $\Delta T$ is obtained from the

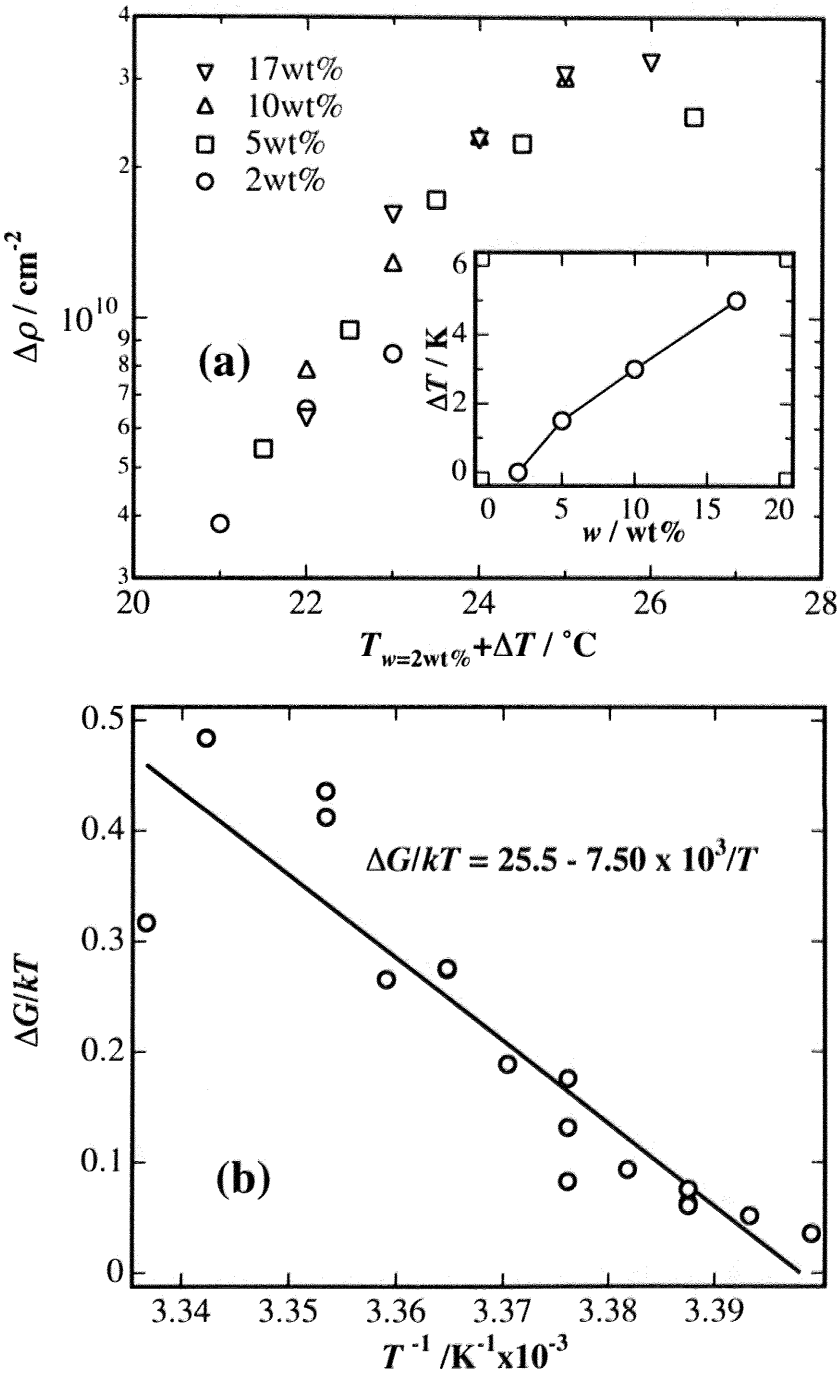


Figure 3.7: (a) Master curve of the scattering-length density, $\Delta\rho$, reduced by the polymer concentration and with a temperature-shift factor, $\Delta T$. The inset shows the concentration dependence of $\Delta T$ . (b) Inverse temperature dependence of the energy of partition of to place EOVE segments in the core, $\Delta E$.

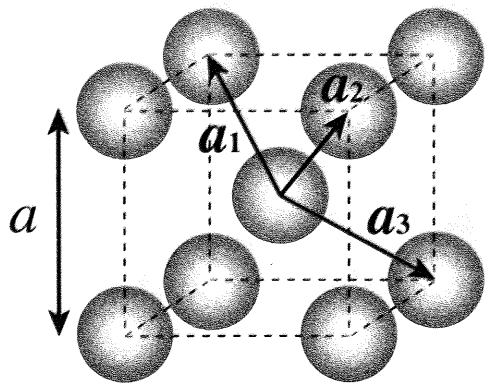


Figure 3.8: Unit cell of the body-centered-cubic lattice and the definition of the principal axes.

inset of Fig. 3.7a,

$$\Delta T \approx 0.29w[\text{wt\%}], 0 \leq w \leq 17\text{wt\%} \tag{3.13}$$

Hence, the partition coefficient is proportional to the polymer concentration in this regime.

### Paracrystal Analysis

In this section, we discuss the scattering peaks appeared in EOVE-*b*-HOVE ($w = 17$ wt%). These peaks indicate formation of macrolattice in the system. The paracrystal theory developed by Hosemann and Bagchi is suitable to describe the structure of macrolattice.[20] The theory introduces the lattice factor, $Z_k$ ($k = 1$, 2, and 3), which is given by

$$Z_k(q) = \frac{1 - |F(q)|^2}{1 - 2|F(q)|\cos(\mathbf{a}_k \cdot \mathbf{q}) + |F(q)|^2} \tag{3.14}$$

where $F(q)$ is the factor relating the degree of distortion,

$$|F(q)| = \exp\left[-\frac{1}{2}\frac{\Delta a^2}{a^2}\left\{(\mathbf{a}_1 \cdot \mathbf{q})^2 + (\mathbf{a}_2 \cdot \mathbf{q})^2 + (\mathbf{a}_3 \cdot \mathbf{q})^2\right\}\right] \tag{3.15}$$

Here, $a$ and $\Delta a$ are the unit cell distance and its standard deviation, respectively. The ratio, $g \equiv \Delta a/a$, is often called the Hosemann's $g$-factor, which determines the order of paracrystallinity. In the case of body centered cubic (bcc) structure, the unit vectors of the principal axes $\mathbf{a}_1$, $\mathbf{a}_2$, and $\mathbf{a}_3$ are defined as shown in Figure 3.8 and the scalar products are given by[21,22]

$$\mathbf{a}_1 \cdot \mathbf{q} = \frac{1}{2}aq(\sin\theta\cos\phi + \sin\theta\sin\phi + \cos\theta)$$

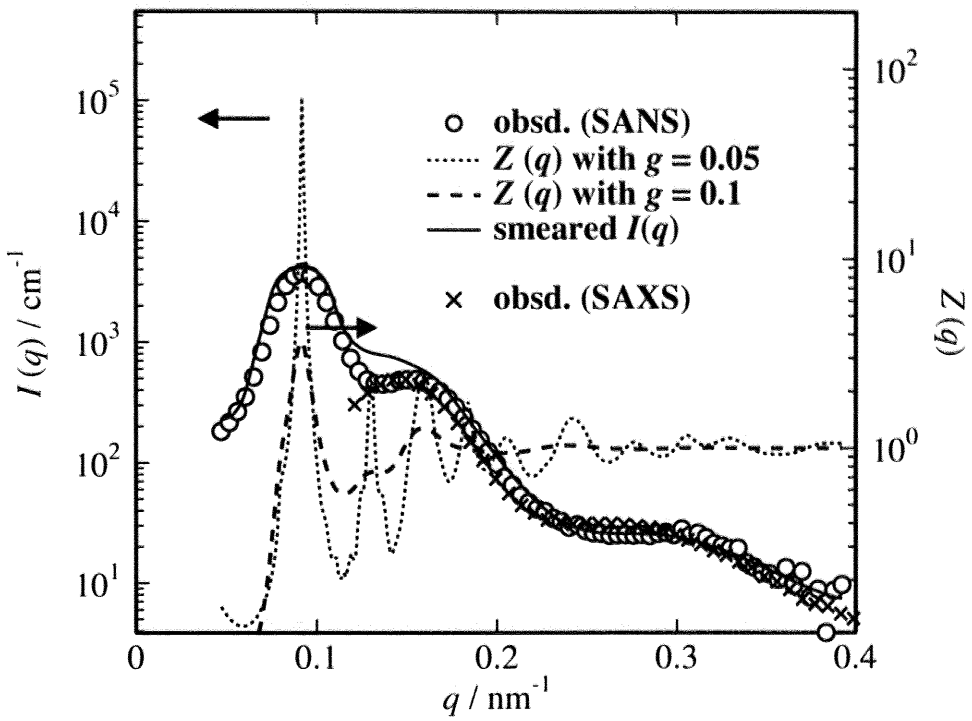


Figure 3.9: Result of curve fitting of the scattering intensity function for EOVE-*b*-HOVE (17 wt%, 26 °C) with the Hosemann-Baguchi's paracrystal theory. Observed SANS function (open circles), the lattice factor $Z(q)$ with $g = 0.05$ (dotted line) and $g = 0.10$ (dashed line), the smeared calculated-SANS function (solid line), and SAXS intensity.

$$\begin{aligned} \mathbf{a}_2 \cdot \mathbf{q} &= \frac{1}{2}aq(-\sin\theta\cos\phi - \sin\theta\sin\phi + \cos\theta) \\ \mathbf{a}_3 \cdot \mathbf{q} &= \frac{1}{2}aq(-\sin\theta\cos\phi + \sin\theta\sin\phi - \cos\theta) \end{aligned} \tag{3.16}$$

Since the macrolattice is randomly oriented in the space, one needs an orientational average as given by,

$$Z(q) = \frac{1}{4\pi}\int_0^{2\pi}\int_0^{\pi} Z_1(q,\theta,\phi)Z_2(q,\theta,\phi)Z_3(q,\theta,\phi)\sin\theta \mathrm{d}\theta\mathrm{d}\phi \tag{3.17}$$

Figure 3.9 shows the result of curve fitting with the paracrystal theory as well as the calculated lattice factor, $Z(q)$, for bcc lattice. The open circles denote the SANS data obtained with an extended camera length of 8 m for EOVE-*b*-HOVE at $w = 17$ wt% at 26 °C. The dot-and-dash line denote the lattice factors, $Z(q)$, with $a = 97.0$ nm for $g = 0.05$ and 0.1, respectively. The solid line denoted the curve-fitted result of the case with $g = 0.1$ by taking account of the smearing of the incident beam width and

the wavelength distribution. Note that a curve fitting with the face-centered-cubic (fcc) lattice model did not work at all. In order to confirm this result, a supplemental study was carried out with small-angle X-ray scattering. The SAXS result is shown with crosses, which is in good agreement with the SANS result. Note that the incident beam width (FWHM) of the SAXS was $\pm 2.04 \times 10^{-4}$ nm$^{-1}$, which is about twice as large as that of the SANS. Therefore, the missing of the second peak of the bcc lattice is due not to the incident beam smearing but to the ill-developed macrolattice of the EOVE-*b*-HOVE, i.e., $g$ ($\approx 0.1$) as was evaluated by curve fitting. According to McConnell et al.,[5,6] block copolymer systems in a selective solvent can take either fcc or bcc packing depending on the length scale of the corona chain length relative to the core dimension. When the corona length is larger than the core size, the system prefers a bcc packing, which is the case in this study.

**Evaluation of the volume fraction of the core and the occupied area on the surface by a single chain**

By knowing the Bragg spacing, $L$, and the radius of the sphere, $R$, the volume fraction of domain can be estimated by the following relationship,

$$L = \frac{a}{\sqrt{2}} = \sqrt{\frac{2}{3}} D_0, \phi_j = \frac{4\pi}{3} j \left(\frac{R}{a}\right)^3 \tag{3.18}$$

where $D_0$ is the nearest neighbor distance, and $j$ is the factor depending on the packing, i.e., $j = 1$ (sc), 2 (bcc), and 4 (fcc). Since we know the EOVE-*b*-HOVE forms a bcc lattice structure, we put $j = 2$ and by substituting $a_{\mathrm{bcc}} = 97.0$ nm and $R = 18.0$ nm on the basis of the data at $w = 17$ wt%, one gets $\phi_{\mathrm{bcc}} = 0.054$. This value is in good agreement with the value ($\phi = 0.056$) evaluated by stoichiometry by assuming perfect exclusion of polyEOVE from others. On the other hand, substitution of $R = 20.0$ nm at $w \leq 10$ wt% leads to an estimation of water content in the spherical domain. It is deduced that about 23 % of the volume of the sphere is occupied by water. In this case, the scattering length density difference, $\Delta\rho$, can be reevaluated by using the value obtained here. The reevaluated value is $3.6 \times 10^{10}$ cm$^{-2}$, which is also in good agreement with the observed one, $3.3 \times 10^{10}$ cm$^{-2}$ (Fig. 3.6). It is of interest to consider the area partitioned to a single chain on the surface of a core of a micelle. The number of block chains in a micelle, $N$, is estimated to

$$N = \frac{V}{Z_{\mathrm{EOVE}} v_{\mathrm{EOVE}}} = 633 \tag{3.19}$$

where $Z_{\mathrm{EOVE}}$ and $v_{\mathrm{EOVE}}$ are the degree of polymerization and monomer volume of EOVE, respectively. Since the surface area of a corona is simply obtained by $S = 4\pi\langle R\rangle^2$, one obtains $(S/N)^{1/2}$ to be

$$\left(\frac{S}{N}\right)^{1/2} = 2.5 \text{ nm} \tag{3.20}$$

Therefore, roughly speaking, an area of $2.5^2$ nm$^2$ is partitioned to each block chain. Interestingly, this value is very close to the surface area occupied by a block polymer chain consisting of PS-PB block copolymer with polystyrene volume fraction being 0.26 in a selective solvent ($(S/N)^{1/2} \sim 2.4$ nm).[3] In the case of lamellar domain structure in a good solvent, the scaling relation is obtained,[1]

$$\left(\frac{S}{N}\right)^{1/2} \sim \phi^{-1/3} \tag{3.21}$$

Unlike to the above case, the $(S/N)^{1/2}$ for EOVE-*b*-HOVE does not depend on the volume fraction of the polymer at least in the concentration range of $2 \leq w \leq 17$ wt%. This may be due to a strong segregation at the surface of core.

### 3.3.3 Sharp Structural transitions with respect to temperature

Figure 3.10 shows the phase diagram of EOVE-*b*-HOVE in aqueous solutions determined by SANS. It consists of three regimes, namely the regimes of (i) molecular mixture, (ii) micelles, and (iii) macrolattice. The solid lines dividing the individual regimes were drawn for the eye. As shown in this phase diagram, the disorder-to-order transition, i.e., from molecular mixture to micelles or macrolattice, is very sharp with respect to temperature and is in the order of sub-degrees of centigrade. In addition, the phase-dividing line seems to be well represented by a monotonically decreasing function with concentration, indicating that the interaction parameter is a linear function of polymer concentration. This fact is in good agreement of the result of the analysis of $I(0)$ in which the contrast factor, $\Delta\rho$, is reduced to a master curve by employing a shift factor varying linearly with temperature (See Fig. 3.7).

Figure 3.11 shows the model of the assembly of EOVE-*b*-HOVE block copolymers in water. At low temperatures, the polymer chains are molecularly dispersed in the solvent. However, by increasing temperature, a micelle formation takes place and polyEOVE chains aggregate themselves in a core. The polyHOVE chains remain as

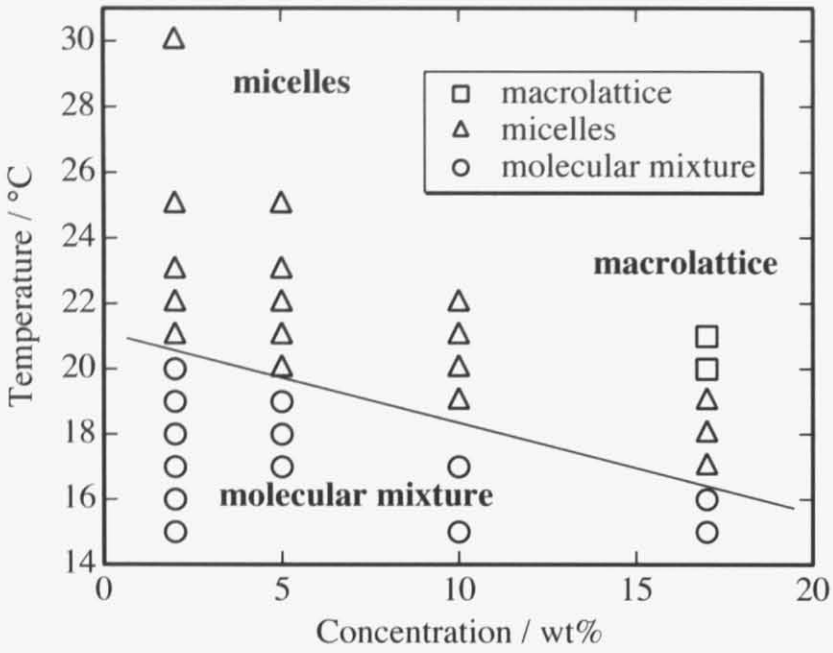


Figure 3.10: Phase diagram of EOVE-*b*-HOVE aqueous solutions, consisting of three phases; molecular mixture, micelles, macrolattice.

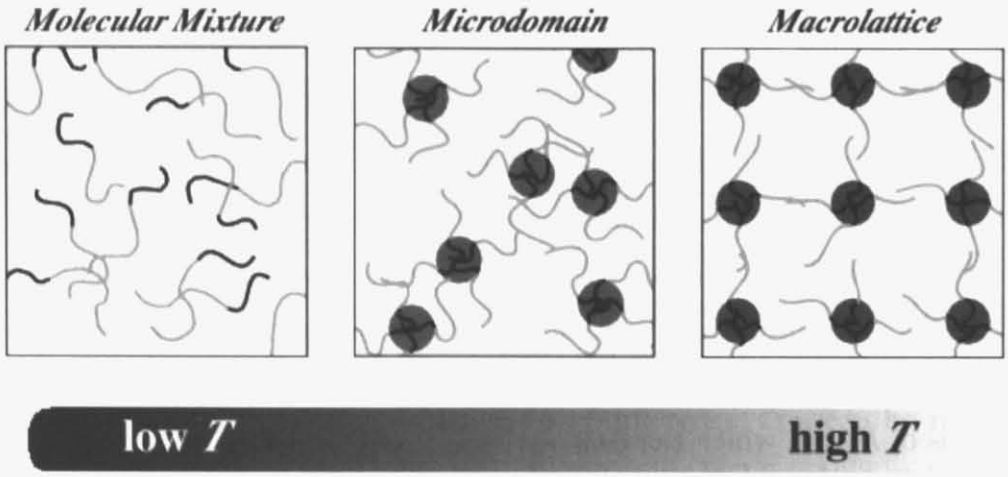


Figure 3.11: Schematic representation of showing two transitions from the molecular mixture (left) to the crystallike structure with macrolattice (right) by way of a micellar structure (middle).

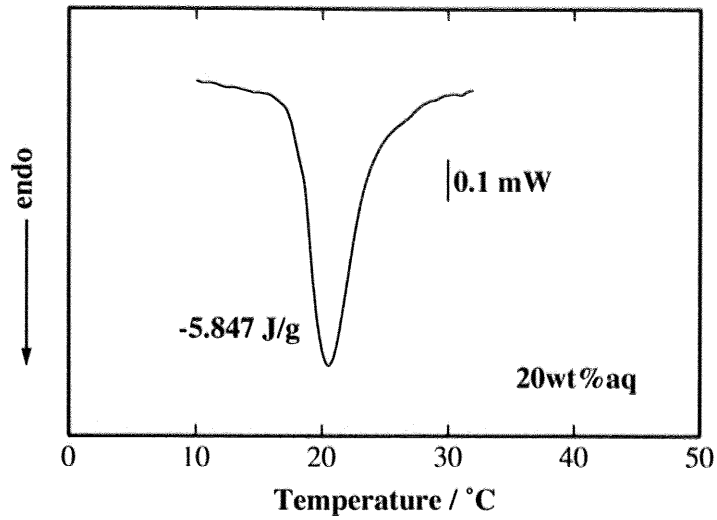


Figure 3.12: DSC thermogram of EOVE-*b*-HOVE aqueous solution with $w = 20$ wt%.

brushes and play as emulsifier or surfactant. However, when the polymer concentration is high enough, morphological transition may take place directly from a molecular mixture to a macrolattice structure. This type of transition is commonly observed in various types of polyampholytes, such as polystyrene-*block*-polyisoprene (PS-*b*-PI) block copolymer[5] and poly(ethylene oxide)-*block*-poly(propylene oxide) (PEO-*b*-PPO).[10] In the case of latter, a lyotropic morphological transition was observed. However, it should be emphasized that the transition of EOVE-*b*-HOVE seems to be much sharper than that of these systems.

### 3.3.4 Origin of the sharp transition

In order to elucidate the sharp disorder-order transition of EOVE-*b*-HOVE in aqueous solutions, a thermal analysis was carried out. Figure 3.12 shows the DSC thermogram of EOVE-*b*-HOVE aqueous solutions with $w = 20$ wt%. As shown in the figure, a sharp endothermic peak was observed around $T = 20$ °C. The enthalpy for hydrophobic dissociation was observed to be $-5.85$ J for 27.3 mg for the solution, which is converted to $\Delta H = -2.05$ kcal/mol-EOVE. This value is about twice as large as that for poly(*N*-isopropylacrylamide) gel in water, i.e., $\Delta H_{\mathrm{NIPA}} = -0.946$ kcal/mol-NIPA (3.95 kJ/mol-NIPA).[23] Note that the value of $\Delta H_{\mathrm{NIPA}}$ itself is in good agreement with those by Otake et al. ($-3.3 \sim -4.5$ kJ/mol-NIPA).28 It should be noted here that

$\Delta H_{\mathrm{NIPA}}$ for PNIPA gels is significantly smaller than that for PNIPA linear polymer solutions, e.g., 6.3 kJ/mol (Schild)[24] and $-4.8 \sim -6.1$ kJ/mol (Otake et al.),[25] which may be ascribed to a lowering of "the degree of hydrophobic hydration" in the gels by introducing the cross-linked structure. Shild assigned this enthalpy change to hydrogen bond interaction.[24] However, as discussed by Shibayama et al.,[23] it seems more reasonable to assign this endotherm as the dissociation enthalpy of the hydrophobic interaction.

The presence of this sharp endotherm around 20 °C clearly indicates that an iceberg melting takes place at this temperature. This causes a drastic change in the intermolecular interaction between EOVE segments and water molecules, resulting in a sharp morphological transition. This transition could be even sharper than a volume phase transition of NIPA gels because a larger endotherm is involved in the EOVE-water system. In the case of van der Waals interacting systems, the interaction parameter is a monotonic function of temperature and thermodynamic transition takes place as a result of the change of a delicate balance of enthalpic and entropic parts of free energy. On the other hand, the disorder-order transition of the EOVE-*b*-HOVE aqueous systems is governed by the enthalpy change due to melting of the iceberg structure, which is the first order transition by the definition of thermodynamics. This is why the transition takes place with in a limited range of temperature irrespective of polymer concentration.

## 3.4 Conclusion

Nano-order structure formation of block copolymers (EOVE-*b*-HOVE) in aqueous systems has been studied by SANS as well as by rheological and thermal analyses. The following facts were disclosed: (1) There exists disorder-order transitions, from a molecular mixture to micelles or a molecular mixture to macrolattice. The latter corresponds to a drastic change in macroscopic flow behavior, such as gelation. A phase diagram was constructed on the basis of the SANS results. (2) At low temperatures, the EOVE-*b*-HOVE block copolymer homogeneously dissolves in water, in which the correlation length $\xi$ is evaluated to be 4.0 to 3.5 nm for 5 and 10 wt%, respectively, at the temperature range studied here. (3) In the micelle regime, the size of core is $18.0 - 20.0$ nm and is hardly dependent on either temperature or polymer con-

centration. (4) At higher temperatures and at higher polymer concentrations, a bcc macrolattice structure is formed with a unit cell of 97.0 nm and radius of 18.0 nm (for $w = 17$ wt%). (5) A master relationship is obtained for the scattering-length density difference, $\Delta\rho$, with a reasonable temperature shift factor, $\Delta T$. This suggests that the scattered intensity is proportional to the polymer concentration. In other words, the micelle structures are rather identical to each other in the micelle phase, irrespective of polymer concentration. The temperature shift factor $\Delta T$ is a linear function of concentration, i.e., $\Delta T = 0.29w$, indicating that the polymer-solvent interaction parameter, $\chi$, is also proportional to polymer concentration. (6) A significant amount of water could be associated in an EOVE core up to 23 wt% in the micelle phase. This water content agrees with the result of scattering-length density difference between the core and the matrix. (7) The surface area partitioned to a single block chain is about 2.5 nm, which is again in good agreement with another block copolymer systems consisting of PS-PB in a selective solvent. (8) The sharp structural transition was explained as a drastic endothermic change of miscibility between EOVE and water by iceberg melting with 2.05 kcal per mole of EOVE monomeric unit.

# References


[1] Shibayama, M.; Hashimoto, T.; Kawai, H. *Macromolecules* 1983, **16**, 1093.

[2] Watanabe, H.; Kotaka, T.; Hashimoto, T.; Shibayama, M.; Kawai, H. J. *Rheology* 1982, **26**, 153.

[3] Shibayama, M.; Hashimoto, T.; Kawai, H. *Macomolecules* 1983, **16**, 16.

[4] Hashimoto, T.; Shibayama, M.; Kawai, H.; Watanabe, H.; Kotaka, T. *Macomolecules* 1983, **16**, 361.

[5] McConnell, G. A.; Gast, A. P. *Macromolecules* 1997, **30**, 435.

[6] McConnell, G. A.; Gast, A. P.; Huang, J. S.; Smith, S. D. *Phys. Rev. Lett.* 1993, **71**, 2102.

[7] Huang, C. I.; Lodge, T. P. *Macromolecules* 1998, **31**, 3556.

[8] Hamley, K. J.; Lodge, T. P.; Huang, C. I. *Macromolecules* 2000, **33**, 5918.

[9] Zhang, L.; Eisenberg, A. *Science* 1995, **268**, 1728.

[10] Alexandridis, P.; Ollson, U.; Lindman, B. *Langmuir* 1998, **14**, 2627.

[11] Aoshima, S.; Hashimoto, K. *J. Polym. Sci. Part A: Polym. Chem.* 2001, **39**, 746.

[12] Aoshima, S.; Sugihara, S. *J. Polym. Sci. Part A: Polym. Chem.* 2000, **38**, 3962.

[13] Sugihara, S.; Aoshima, S. *Koubunshi Ronbunshu* 2001, S. **58**, 304.

[14] Sugihara, S.; Matsuzono, S.; Sakai, H.; Abe, M.; Aoshima, S. *J. Polym. Sci. Part A: Polym. Chem.* 2001, **39**, 3190.

[15] Aoshima, S.; Higashimura, T. *Macromolecules* 1989, **22**, 1009.

[16] Aoshima, S.; Oda, H.; Kobayashi, E. *J. Polym. Sci. Part A: Polym. Chem.* 1992, **30**, 2407.

[17] Schwahn, D.; Takeno, H.; Willner, L.; Hasegawa, H.; Jinnai, H.; Hashimoto, T.; Imai, M. *Phys. Rev. Lett.* 1994, **73**, 3427.

[18] Hashimoto, H.; Fujimura, M.; Hashimoto, T.; Kawai, H. *Macromolecules* 1981, **14**, 844.

[19] de Gennes, P. G. *Scaling Concepts in Polymer Physics* Cornell University: Ithaca, 1979.

[20] Hosemann, R.; Bagchi, S. N. *Direct Analysis of Diffraction by Matter* North-Holland: Amsterdam, 1962.

[21] Matsuoka, H.; Tanaka, H.; Hashimoto, T.; Ise, N. *Phys. Rev. B* 1987, **36**, 1754.

[22] Matsuoka, H.; Tanaka, H.; Iizuka, N.; Hashimoto, T.; Ise, N. *Phys. Rev. B* 1990, **41**, 3854.

[23] Shibayama, M.; Mizutani, S.; Nomura, S. *Macromolecules* 1996, **29**, 2019.

[24] Shild, H. G. *Prog. Polym. Sci.* 1992, **17**, 163.

[25] Otake, K.; Inomata, H.; Konno, M.; Saito, S. *Macromolecules* 1990, **23**, 283.

# Chapter 4

# Heat-induced Self-assembling of Thermosensitive Block Copolymer / DLS Study

## 4.1 Introduction

In the previous chapter, we studied structural transitions of poly(2-ethoxyethyl vinyl ether)-*block*-poly(2-hydroxyethyl vinyl ether) (EOVE-*b*-HOVE) in aqueous solutions. One of the fascinating phenomena was a thermoreversible sol-gel transition around 20 °C observed in a 17 wt% EOVE-*b*-HOVE aqueous solution. The viscosity of the solution changed more than four orders of magnitude within a few degree of Celsius. It was found by a series of SANS experiments that this rheological transition is due to morphological transition from a molecular dispersion to a macrolattice structure with a body-centered-cubic structure. Though the SANS study also indicated presence of an intermediate state with micellar structure, it was not decisive because of the limitation of the spatial resolution of SANS.

In this chapter, the dynamics and rheological properties of EOVE-*b*-HOVE aqueous solutions as a function of temperature and concentration are reported. And the models of morphological transitions proposed in the previous chapter will be confirmed.

## 4.2 Theoretical Background

The dynamics of polymer solutions can be analyzed by dynamic light scattering (DLS). Let us first define the normalized first order correlation function for the scat-

tered electric field $g^{(1)}(\mathbf{q},t)$ from the sample, where $\mathbf{q}$, $t$ are the scattering vector and time, respectively. $g^{(1)}(\mathbf{q},t)$ is given as follows,[1]

$$g^{(1)}(\mathbf{q},\tau) = \frac{\langle E(\mathbf{q},\tau)E^*(\mathbf{q},t+\tau)\rangle}{\langle |E(\mathbf{q},\tau)|^2\rangle} = \frac{\langle E(\mathbf{q},0)E^*(\mathbf{q},\tau)\rangle}{\langle |E(\mathbf{q},0)|^2\rangle} \tag{4.1}$$

where $E(\mathbf{q},t)$ is the scattering field and $E^*(\mathbf{q},t)$ is the complex conjugate of $E(\mathbf{q},t)$. In a DLS measurement, we obtain the second-order correlation function, $g^{(2)}(\mathbf{q},\tau)$, which is the intensity-intensity-time correlation function defined by

$$g^{(2)}(\mathbf{q},\tau) = \frac{\langle I(\mathbf{q},0)I(\mathbf{q},\tau)\rangle}{\langle |I(\mathbf{q},0)|^2\rangle} = \frac{\langle E(\mathbf{q},0)E^*(\mathbf{q},0)E(\mathbf{q},\tau)E^*(\mathbf{q},\tau)\rangle}{\langle |E(\mathbf{q},\tau)|^2\rangle} \tag{4.2}$$

Here, $I(\mathbf{q},t)$ is the scattered intensity at $\mathbf{q}$ and at time $t$. The two correlation functions are linked via Siegert relation,[2,3] i.e.,

$$g^{(2)}(q,\tau) = 1 + |g^{(1)}(q,\tau)|^2 \tag{4.3}$$

In general, there are many relaxation processes, and $g^{(1)}(\mathbf{q},\tau)$ is given with the decay-rate distribution function, $G(\Gamma)$, where $\Gamma$ is the decay rate,

$$g^{(1)}(q,\tau) = \int_0^\infty G(\Gamma)\exp(-\Gamma\tau)\mathrm{d}\Gamma \tag{4.4}$$

For example, if the scattering medium has two relaxation modes with monodisperse distributions, $g^{(1)}(\mathbf{q},\tau)$ is simply given as a sum of two exponential functions, i.e.,

$$g^{(1)}(q,\tau) = A\exp(-\Gamma_1\tau) + (1-A)\exp(-\Gamma_2\tau) \text{ (two exponentials)} \tag{4.5}$$

$\Gamma_i$ ($i = 1, 2$) is the characteristic decay rate related to the diffusion coefficient, $D_i$, as follows

$$\Gamma_i = D_i q^2 \tag{4.6}$$

Rigorously speaking, eq. 4.6 is valid only at infinite dilution. In reality, motion of diluent, i.e., the solvent has to be taken into account as follows,[4,5]

$$\Gamma = (1-\phi)^2 Dq^2 \tag{4.7}$$

The values of the hydrodynamic radius related to the $i$-th mode, $R_{\mathrm{H},i}$, can be evaluated with the relation below.

$$R_{\mathrm{H},i} = \frac{kT}{6\pi\eta_0 D} = \frac{kTq^2}{6\pi\eta_0\Gamma_i} \tag{4.8}$$

Here, $k$ is Boltzmann constant and $\eta_0$ is the solvent viscosity at temperature $T$.

The above discussion is valid for ergodic medium, where time average is equal to ensemble average. Most of polymeric systems can be regarded as ergodic medium. However, polymer gels have nonergodicity due to immobilization of polymer chains introduced by cross-linking as extensively discussed in the literature.[6-9] In the case of a nonergodic medium, the scattered intensity, $I(q)$, varies with sample position because of the lack of ergodicity. Hence, two types of averaging have to be defined to describe the system, i.e., the time average, $\langle I(q)\rangle_T$, and ensemble average, $\langle I(q)\rangle_E$. The intensity distribution, $P(\langle I(q)\rangle_T)$ , obeys the following relationship,[7]

$$P\left(\langle I(q)\rangle_T\right) = H\left[\langle I(q)\rangle_T - I_F(q)\right] \exp\left[-\frac{\langle I(q)\rangle_T - I_F(q)}{\langle I(q)\rangle_E - I_F(q)}\right] \tag{4.9}$$

where $I_F(q)$ is the dynamic component in the scattered intensity, $\langle I(q)\rangle_T$, and $H(x)$ is the Heaviside function, i.e., $H(x) = 0$ for $x < 0$ and $H(x) = 1$ for $x \geq 1$.

## 4.3 Experimental Section

### 4.3.1 Sample

The procedure for synthesis of EOVE-*b*-HOVE was described in the previous chapter. In addition, the corresponding homopolymers, i.e., polyEOVE and polyHOVE, were also prepared for comparison. The details of synthesis were reported elsewhere.[10,11] Prescribed amount of EOVE-*b*-HOVE was dissolved in deuterated water ($D_2O$). It should be noted that there exists a significant isotope effect in phase behavior in polymer blends[12,13] as well as in polymer gels.[14] Therefore $D_2O$ was chosen as a solvent instead of $H_2O$ even for dynamic light scattering measurement (DLS). The sample solutions were filtered with 0.20 $\mu$m milipore filter.

### 4.3.2 DLS

Dynamic light scattering (DLS) experiments were carried out on a static/dynamic compact goniometer (SLS/DLS-5000), ALV, Langen, Germany. A He-Ne laser with 22 mW was used as the incident beam. Non-ergodic DLS measurements were conducted with a rotation attachment, ALV, at a fixed angle of 90 °. Typical measuring time was 30 s. The temperature of the sample was regulated within an error of ±0.1 °C.

### 4.3.3 Rheological measurements

A stress-control-type rheometer (Carri-Med CSL2 100, TA-Instruments) was used to measure the flow properties and dynamic viscoelasticity of the polymer solutions. A cone-plate with a diameter of 4 cm and an angle of 2 ° was employed. In the case of flow property measurements, after stress was given to the sample within 3 min, and reduced within 3 min, the flow curve was obtained. The shear storage modulus $G'$ and loss modulus $G''$ were measured as a function of frequency, $f$. Depending on the viscoelastic properties, a suitable shear amplitude, $\gamma$, was chosen to ensure the linearity of dynamic viscoelasticity. The temperature of the samples was controlled within 0.1 °C by means of a Peltier element.

## 4.4 Results and discussion

### 4.4.1 Rheological behavior

Figure 4.1 shows dynamic mechanical behavior of EOVE-*b*-HOVE aqueous solutions at polymer concentrations of 20 wt%. As shown in the figure, both the storage, $G'$, and loss moduli, $G''$, increased rapidly at 20 °C. This is due to micellization of polyEOVE due to its strong hydrophobicity, followed by a macrolattice formation as evidenced in the previous chater.[10] The polyHOVE chains anchored to different micelles interpenetrating to each other, resulting in a drastic increase in viscosity of the system. Figure 4.2 shows flow curves of EOVE-*b*-HOVE aqueous solutions of 15 wt% at 15.0, 20.5, and 21.0 °C. Surprisingly enough, the change in viscoelasticity is remarkably sharp with respect to temperature. The flow behavior changes within a very limited temperature range, i.e., $19 < T < 20$ °C, from Newtonian flow ($T < 19$ °C), to non-Newtonian ($T \approx 20.5$ °C), and plastic flow behavior ($T > 21$ °C). In the Newtonian flow region, the shear stress, $\sigma$, is proportional to the shear rate, $\mathrm{d}\gamma/\mathrm{d}t$, as follows,

$$\sigma = \eta \frac{\mathrm{d}\gamma}{\mathrm{d}t} \tag{4.10}$$

and the viscosity $\eta = 0.0544$ Pa·s. This means that the system is a homogeneous polymer solution. In the non-Newtonian region ($T \approx 20.5$ °C), on the other hand, the flow behavior suggests that there exists a heterogeneous structure, such as micelles with long hair chains interpenetrating to each other. On the other hand, the rheolog-

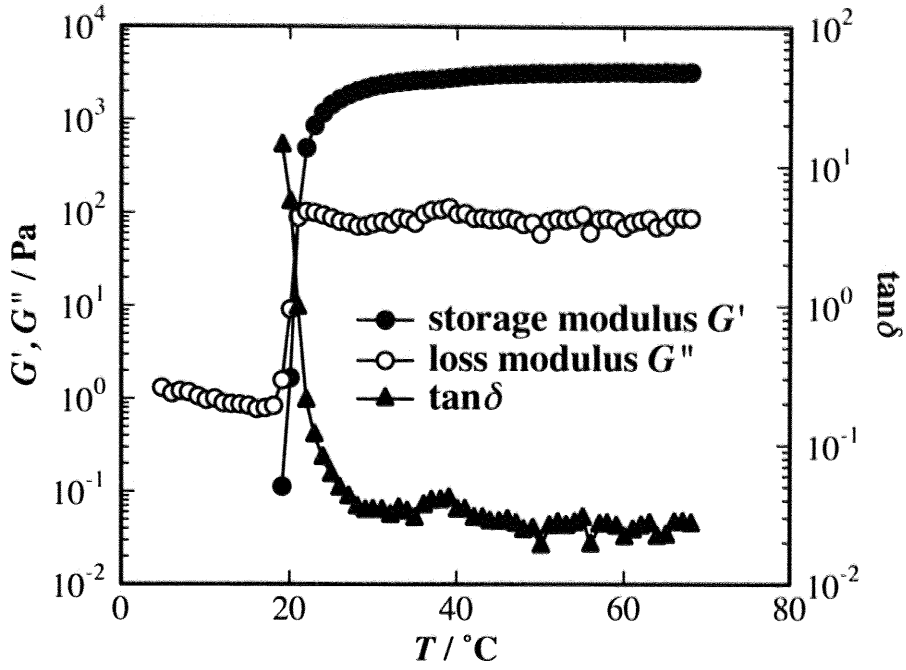


Figure 4.1: Dynamic mechanical behavior of EOVE-*b*-HOVE block copolymer solution at 20 wt% (frequency = 1Hz). $G'$; storage and $G''$; loss moduli, and $tan\delta$ ; loss tangent

ical behavior in the plastic flow region indicates the presence of a solid-like structure responsible for a yield stress. The flow behavior was given in the following form,

$$\sigma \cong \sigma_0 + \eta_a \frac{d\gamma}{dt} \tag{4.11}$$

with the yield stress $\sigma_0$ = 45.0 Pa and the apparent viscosity $\eta_a$ = 0.140 Pa·s in this particular case. Another interesting feature is absence of significant hysteresis even in the region of the plastic flow. Similar rheological transitions were observed in polystyrene-*block*-polybutadiene in a selective solvent (e.g., n-tetradecane; C14).[15,16] It should be noted here, however, the transition of EOVE-*b*-HOVE aqueous solutions is much sharper than that of polystyrene-*block*-polybutadiene in C14.

Figure 4.3 shows the frequency, $f$, dependence of $G'$ and $G'$ of EOVE-*b*-HOVE aqueous solutions at various temperatures. At $T$ = 19.5 °C, $G'$ and $G''$ exhibit typical behavior for viscoelastic (Maxwellian) fluids. That is, $G'$ scales with $f^2$ and $G''$ does $f^1$. At the sol-gel transition threshold, it is known that $G'$ and $G''$ becomes collinear with $f$.[17,18] As a matter of fact, the dynamic mechanical behavior shows $G'$ and $G' \sim f^{1/2}$ for $f > 1$ Hz at $T$ = 21.0 °C. It is interesting that the $G'$ and $G''$ functions

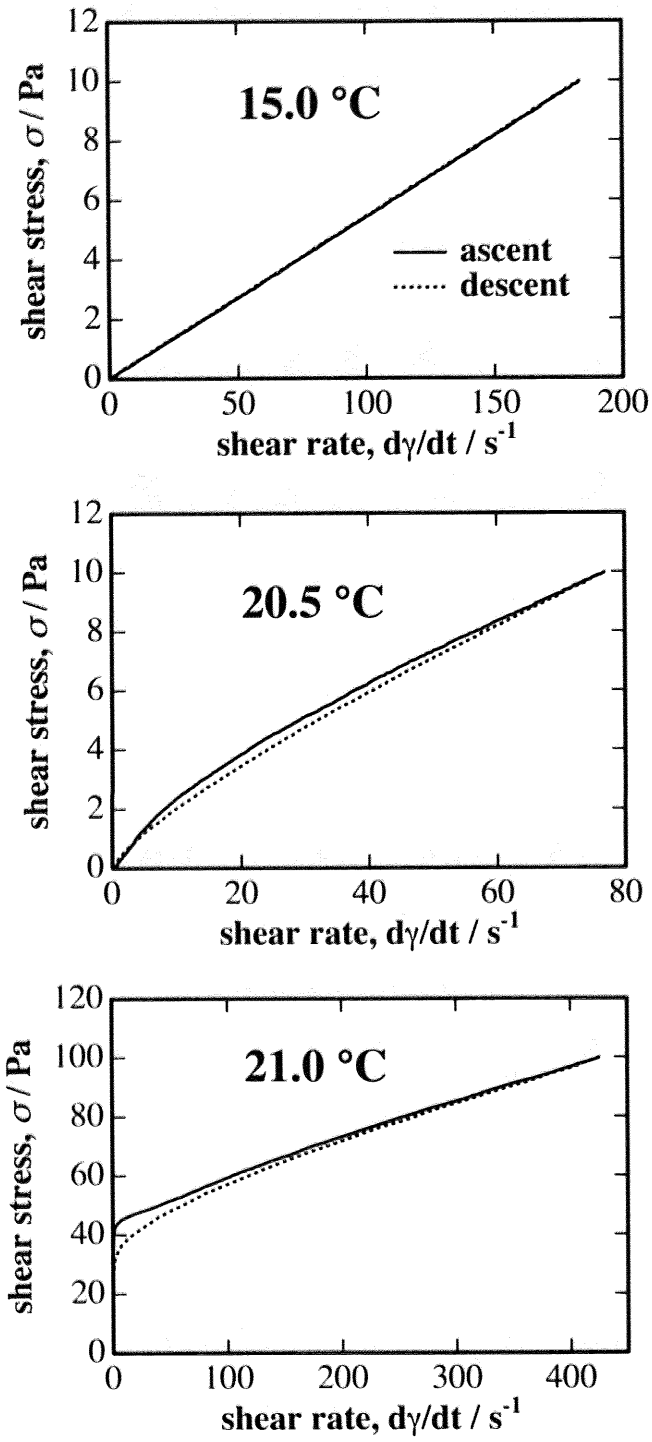


Figure 4.2: Flow behaviors of EOVE-*b*-HOVE in 15 wt% aqueous solution at various temperatures.

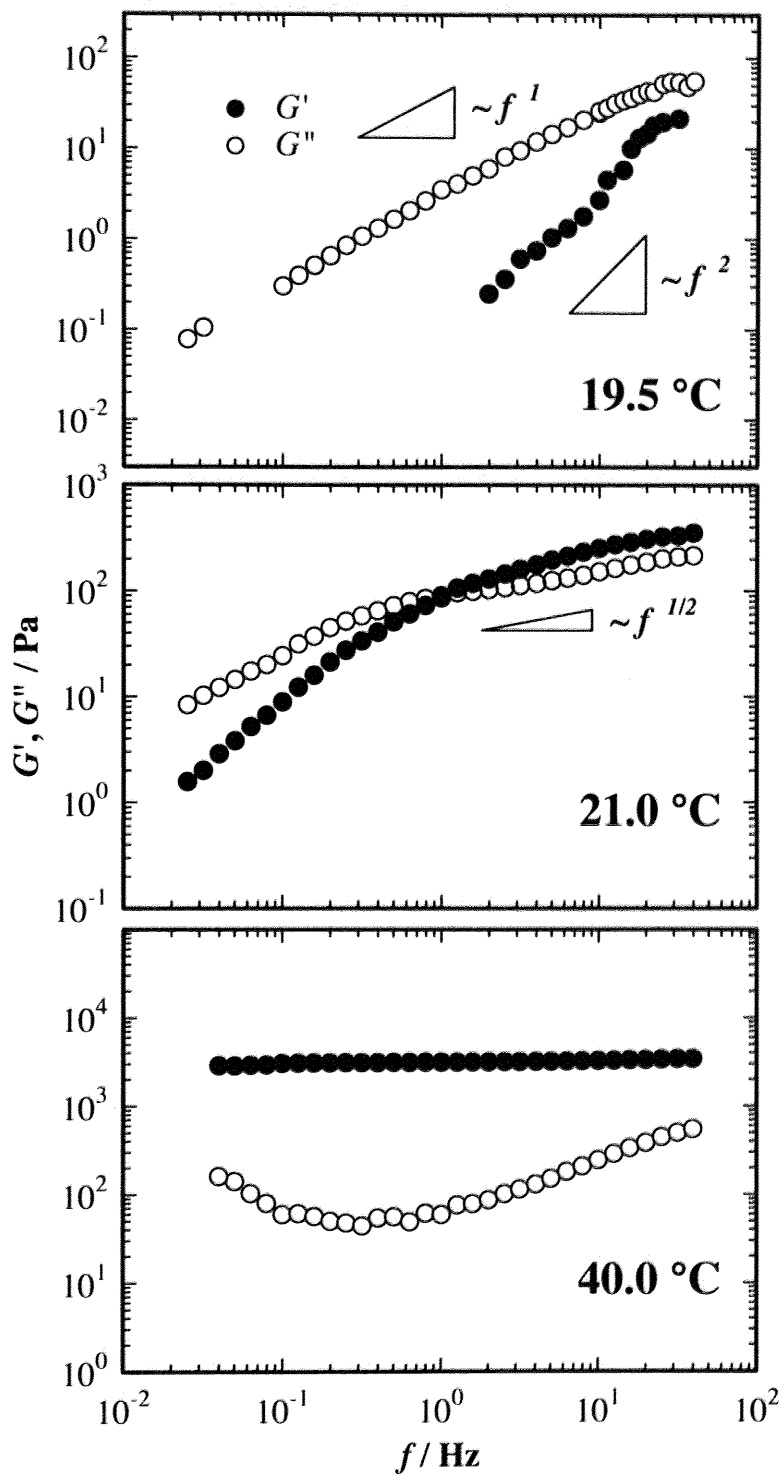


Figure 4.3: Viscoelastic behaviors of EOVE-*b*-HOVE in 20 wt% aqueous solution at various temperatures.

crossover at $f \approx 1$ Hz. This indicates that this system becomes a viscoelastic fluid with a long relaxation time at this frequency. At a higher frequency than this critical frequency, i.e., $f_c \approx 1$ Hz, the system behaves as a gel. However, for $f < f_c$, it is a viscous solution and flows. At a temperature above the sol-gel transition, both $G'$ and $G''$ become frequency independent as a typical elastic matter does. In addition, $G'$ is more than one order of magnitude larger than $G''$ in this frequency region, indicating that the loss tangent, $\tan\delta$, is less than 0.1. All of these results on rheological properties support structural transition from a non-structured polymer solution to a macrolattice structure by way of sol-gel transition.

### 4.4.2 DLS results

#### Homopolymers

Figure 4.4 shows (a) correlation functions (CFs), $g^{(2)}(\tau) - 1$, and (b) cluster distribution functions (CDs), $G(\Gamma)$, of polyHOVE in aqueous solution at various temperatures. The polymer concentration was 1.0 wt%. The CF shows existence of single relaxation corresponding to the translational diffusion of polyHOVE chains. The characteristic decay time, $\Gamma^{-1}$, shifted toward shorter relaxation time. However, this does not mean a contraction of polyHOVE chains but this is due to a decrease in the solvent viscosity with increasing temperature. The variation of $R_H$ with temperature will be discussed in conjunction with that of polyEOVE.

Figure 4.5 shows (a) CFs and (b) CDs, of polyEOVE in aqueous solution at various temperatures. Because the scattered intensity was very weak, the concentration was increased to 2.0 wt% instead of 1.0 wt%. In contrast to the case of polyHOVE, CFs seem to be strongly temperature dependent. Note that there are two peaks in the CDs, i.e., the first, $\Gamma_{\text{fast}}^{-1}$ ($\equiv \Gamma_1^{-1}$), and slow modes, $\Gamma_{\text{slow}}^{-1}$ ($\equiv \Gamma_2^{-1}$). With increasing temperature, $\Gamma_{\text{fast}}^{-1}$ shifts toward shorter relaxation time and its peak height decreased. On the other hand, $\Gamma_{\text{slow}}^{-1}$ moved toward longer relaxation time and the height increased. These correspond to the translational diffusion of individual polyEOVE chains and clustered polyEOVE chains, respectively. The cluster of polyEOVE chains is deduced to be stable enough to keep their size while individual chains have freedom to attach to or detatch from the cluster. Hence, a dynamic equilibrium of the cluster size distribution exists. This is because the clusters are still

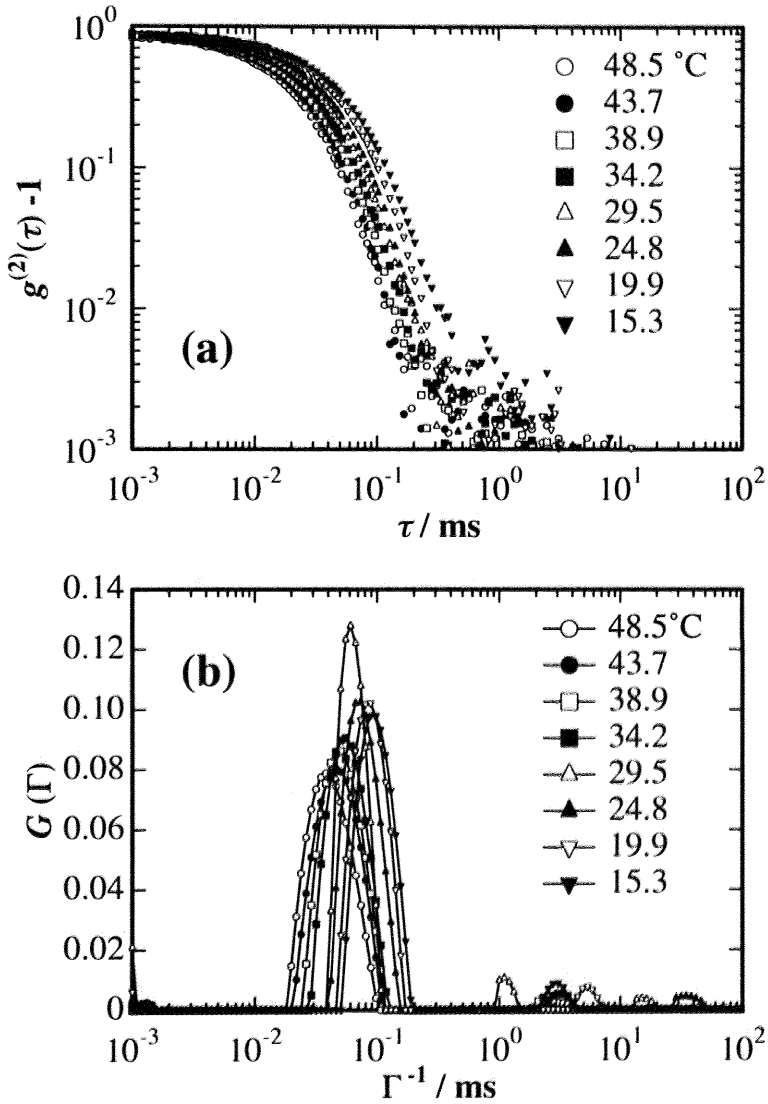


Figure 4.4: (a) CFs and (b) CDs of polyHOVE in aqueous solution at various temperatures.

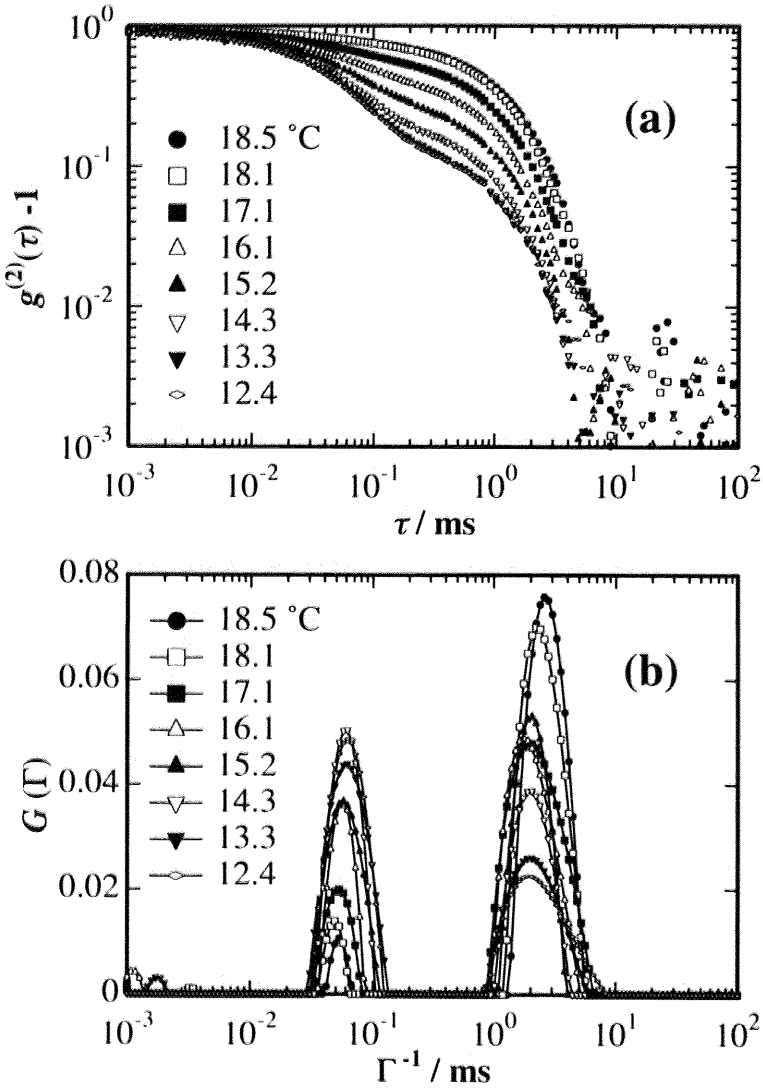


Figure 4.5: (a) CFs and (b) CDs of polyEOVE in aqueous solution at various temperatures. Two relaxation modes appeared assigned to be the fast and slow modes.

soluble in water.

Figure 4.6 shows the variations of (a) $R_H$ of polyHOVE, $R_{H,HOVE}$, (b) $R_H$s of polyEOVE, i.e., $R_{H,EOVE,fast}$ and $R_{H,EOVE,slow}$. Here, the value of $R_{H,HOVE}$ was evaluated with two methods, i.e., from the CONTIN[19,20] analysis (filled circles) and from the cumulant method (open circles). Both results were in good agreement as shown in the figure. This was the case where only single relaxation mode appeared. However, in the following analysis, the CONTIN analysis (i.e., with eq. 4.4) exclusively employed because of the presence of multiple relaxation modes which interfered the cumulant analysis. $R_{H,HOVE}$ was rather temperature independent and was about 6.0 nm. In the case of polyEOVE, on the other hand, $R_{H,EOVE,fast}$ decreased with $T$, while $R_{H,EOVE,slow}$ was a strong function of $T$, particularly for $T \geq 17$ °C. These data indicate that (1) polyHOVE chains are molecularly dispersed in aqueous solutions at 1 wt% irrespective of temperature and (2) polyEOVE chains are in two states, i.e., in molecular dispersion with $R_{H,EOVE,fast} \approx 3.6$ nm and in clustered state. The size of the clusters, $R_{H,EOVE,slow}$, increased with increasing temperature, particularly for $T \geq 18$ °C. This is due to the fact that the lower critical solution temperature (LCST) of polyEOVE in water is located at $T \approx 20$ °C. The invariance of $R_{H,EOVE,fast}$ of polyEOVE indicates that contraction does not take place except for the temperature region near LCST, i.e., $T > 18$ °C.

Figure 4.7 shows the variations of scattered intensity, $I(\theta = 90°)$, for (a) 1.0 wt%-polyHOVE and (b) 2.0 wt%- polyEOVE solutions, where $\theta$ is the scattering angle. As shown in the figure, $I(\theta = 90°)$ of polyHOVE was temperature independent, while that of polyEOVE dramatically increased for $T \geq 17$ °C. These temperature dependence of $I(\theta = 90°)$ also indicates that partial clustering takes place exclusively for polyEOVE above 17 °C.

### EOVE-*b*-HOVE

Figure 4.8 shows (a) CFs and (b) CDs of 1.0 wt% EOVE-*b*-HOVE in aqueous solution during a heating process. The temperature was increased stepwise after 30 second measurement and was paused at least 30 min before next measurement. Though more than 30 CFs were obtained as a function of temperature, only several representative curves are shown in the figure. Similarly to the case of polyEOVE, there exists two relaxations, one around $\Gamma_{fast}^{-1} \approx 0.1$ ms and the other at $1 \leq \Gamma_{slow}^{-1} \leq 6$ ms at $T = 12.6$

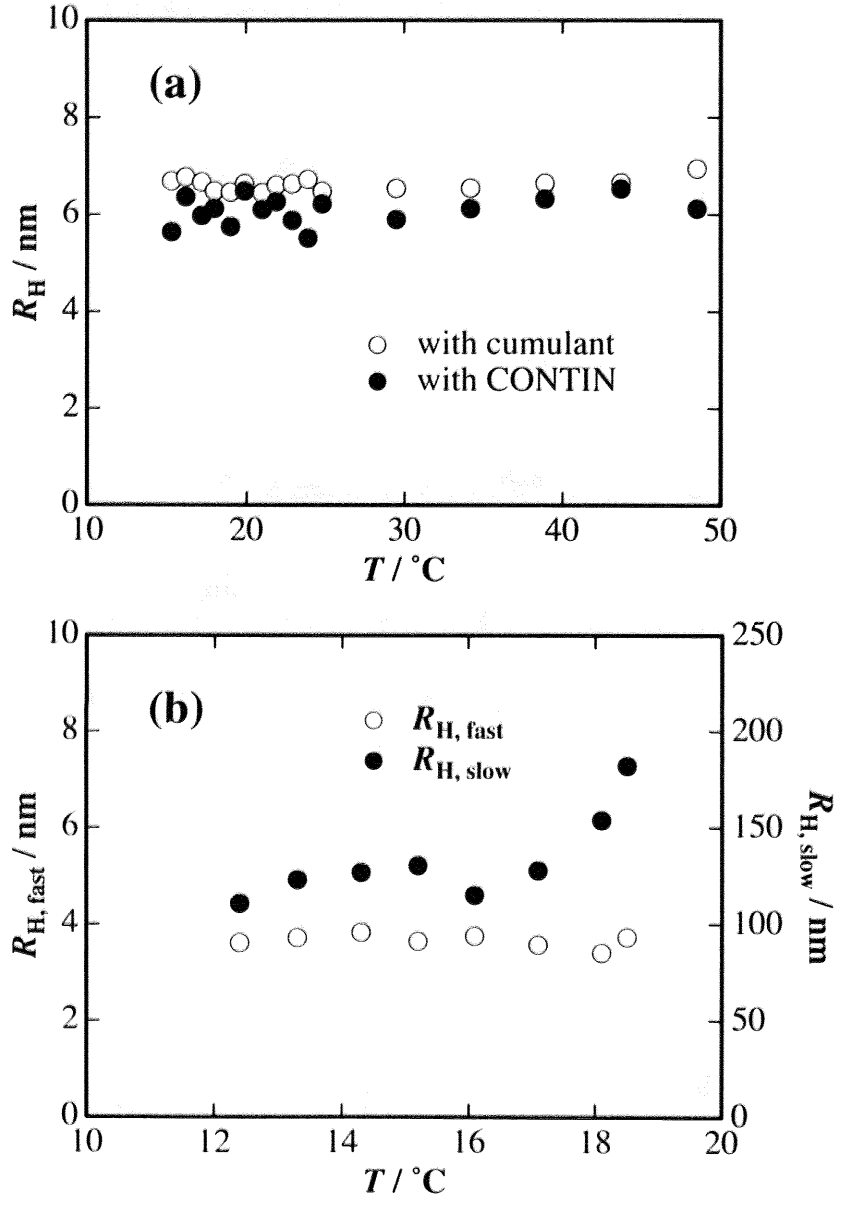


Figure 4.6: Temperature dependence of (a) $R_{\mathrm{H}}$ for polyHOVE (filled circles), and (b) $R_{\mathrm{H,fast}}$ (open circles) and $R_{\mathrm{H,slow}}$ (filled circles) for polyEOVE. The values of $R_{\mathrm{H}}$ for polyHOVE were also determined with the cumulant method (open circles).

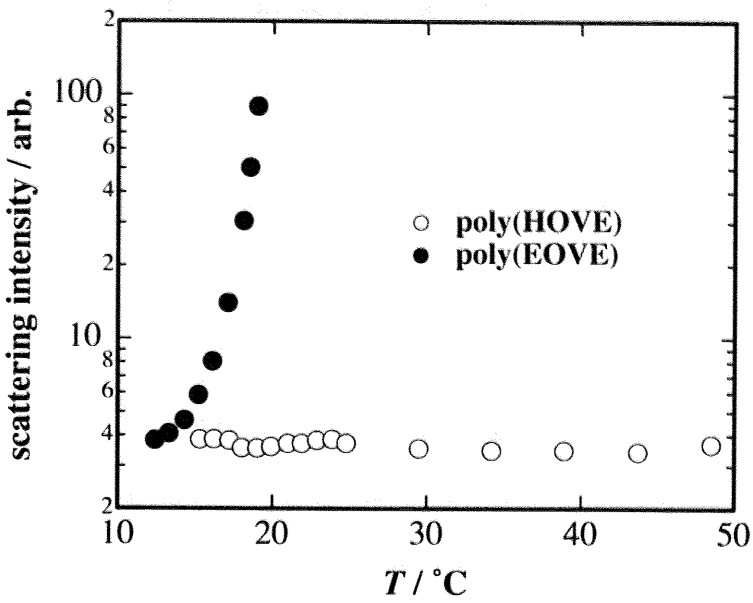


Figure 4.7: Temperature dependence of $I(\theta = 90\ ^{\circ})$s for polyHOVE and polyEOVE aqueous solutions.

°C. The peak position and height at $\Gamma_{\text{fast}}^{-1}$ decreases with increasing $T$, while the position, $\Gamma_{\text{slow}}^{-1}$, of the slow mode was rather strange. At first, $\Gamma_{\text{slow}}^{-1}$ moves toward longer relaxation time. However, $\Gamma_{\text{slow}}^{-1}$ becomes smaller by further increasing $T$ (for $T > 21$ °C). Note that for $T > 21$ °C, the fast mode disappears and the only slow mode survives.

Figure 4.9 shows (a) the variation of $R_{\text{H,fast}}$ and $R_{\text{H,slow}}$ and (b) $I(\theta = 90°)$ of 1.0 wt%- EOVE-*b*-HOVE with $T$. This indicates that micellization took place by anchoring polyEOVE chains to a micelle core. As a result, RH,fast decreased and disappeared by increasing $T$, while $R_{\text{H,slow}}$ increased up to $T = 21.0$ °C and then decreased. The decrease of $R_{\text{H,slow}}$ is ascribed to formation of stable micelles of ca. 80 nm large in radius including polyHOVE corona. In our previous chapter with SANS, the core radius was evaluated to be ca. 20 nm. Hence, this size seems to be consistent with the SANS result.[10] The increase in $R_{\text{H,slow}}$ in the temperature region of $18 < T < 21$ °C is deduced to be a transition region from molecular dispersion to micelles, e.g., interconnected chain like structure as will be discussed later. The variation of $I(\theta = 90°)$ also indicates such transition with $T$. That is, the larger the scattering objects, the larger the scattered intensity. Figure 4.9b also shows that this

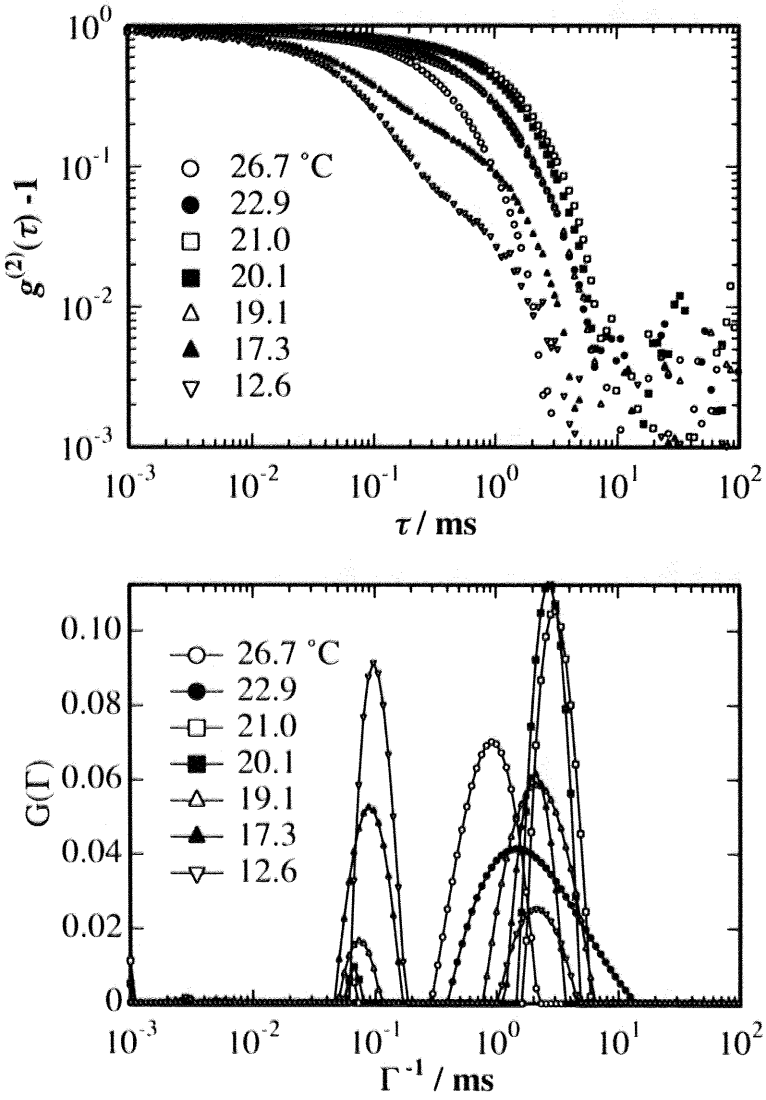


Figure 4.8: (a) CFs and (b) CDs of 1.0 wt% EOVE-*b*-HOVE in aqueous solution.

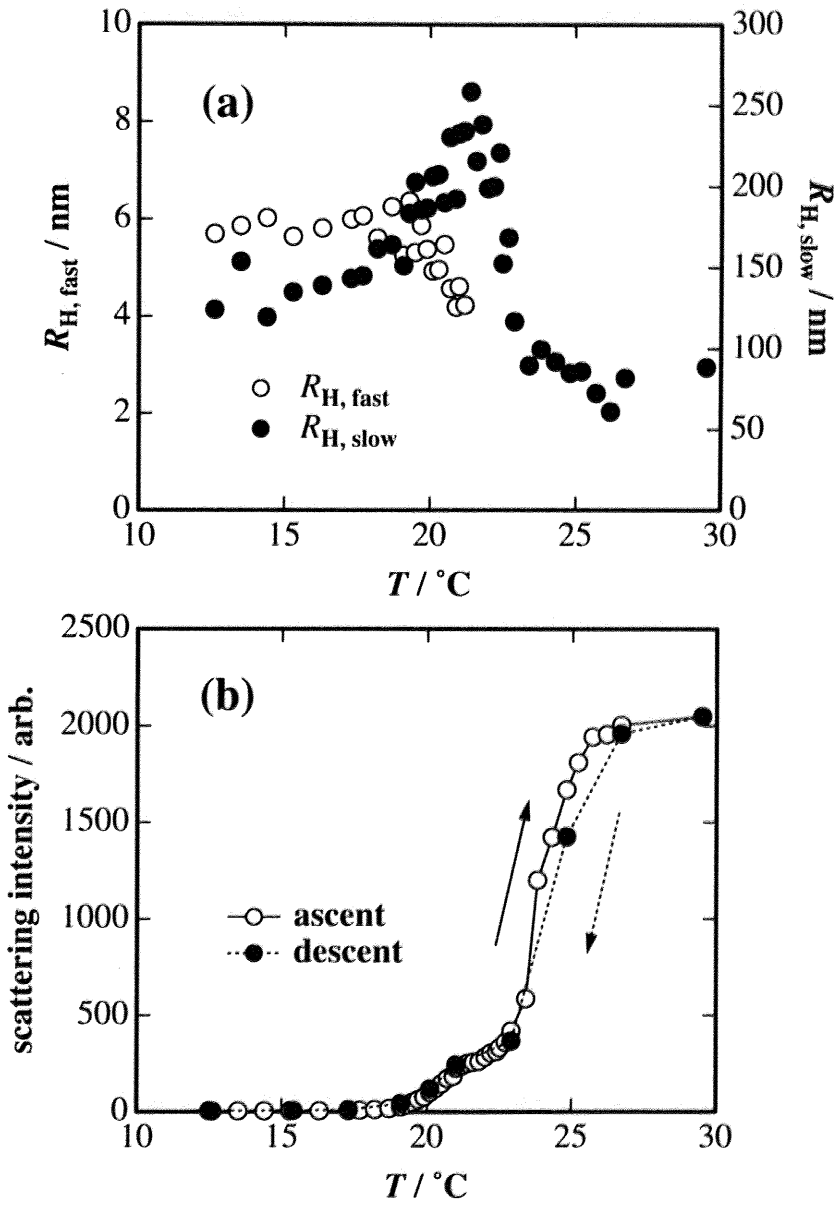


Figure 4.9: Variation of (a) $R_{\mathrm{H,fast}}$, $R_{\mathrm{H,slow}}$ and (b) $I(\theta = 90\ ^{\circ})$ of 1.0 wt% EOVE-*b*-HOVE with $T$.

structure transition is thermo-reversible without significant hysteresis.

Figure 4.10 shows (a) CFs and (b) CDs of 17 wt% EOVE-*b*-HOVE in aqueous solution during a heating process. The scattering angle was 90 °. Different from the case of 1 wt%- EOVE-*b*-HOVE, the CFs exhibits only a slow mode at $\Gamma^{-1} \approx 10^2$ ms for $T \leq 17$ °C. Around 19 °C, CD splits to two peaks, i.e., fast and slow modes. The slower mode is seen at $\Gamma^{-1} \approx 10^2$ ms, while the fast mode is $\Gamma^{-1} \approx 10^1$ ms or less. Another interesting feature observed in Figure 4.10 is the suppression of the initial amplitude of CFs, i.e., $g^{(2)}(\tau = 0) - 1$, for $T > 20.0$ °C. This is an indication of sol-gel transition.[8]

Figure 4.11 shows the peak shift of the CDs shown in Figure 4.10b. This figure clearly indicates that the appearance of the fast mode. With increasing temperature, $\Gamma^{-1}$ decreased gradually. However, at $T = 19.0$ °C, the peak splits to two, as assigned to be the fast and slow modes. The fast mode kept decreasing to the time range of $\Gamma^{-1} \approx 1$ ms or less, which is of the same order of the so-called "gel-mode".[21] Hence, it is deduced that the drastic change of the dynamical property corresponds to the sol-gel transition of the system. As a matter of fact, the 17 wt% EOVE-*b*-HOVE aqueous solution exhibited a characteristic flow behavior with a finite value of yield stress, $\sigma_0$, at temperatures for $T \geq 21$ °C as shown in Figure 4.2. In other words, a concentrated EOVE-*b*-HOVE solution has a plastic behavior at high temperatures.

In order to categorize the fast and slow modes, CFs were obtained by varying the scattering angle. Figure 4.12 shows $G(\Gamma^{-1})$ vs $\Gamma^{-1}q^2$ plots of 17 wt% EOVE-*b*-HOVE aqueous solution at (a) 15.0 °C, (b) 20.2 °C, and (c) 21.0 °C. At $T = 15.0$ °C, a single peak appears and it shifts toward a lower value of $\Gamma^{-1}q^2$ by increasing $q$. On the other hand, at 20.2 °C, which corresponds to the micelle region, there appear two peaks and they are superimposed to each other irrespective of $q$. At 21.0 °C, the peak shift even lower value of $\Gamma^{-1}q^2$, but the peaks are again superimposed irrespective of $q$. Note that the appearance of many peaks is ascribed to the low dynamic correlation by entering a gel phase. This is related to the nonergodic nature of gel phase as will discussed in the next section.

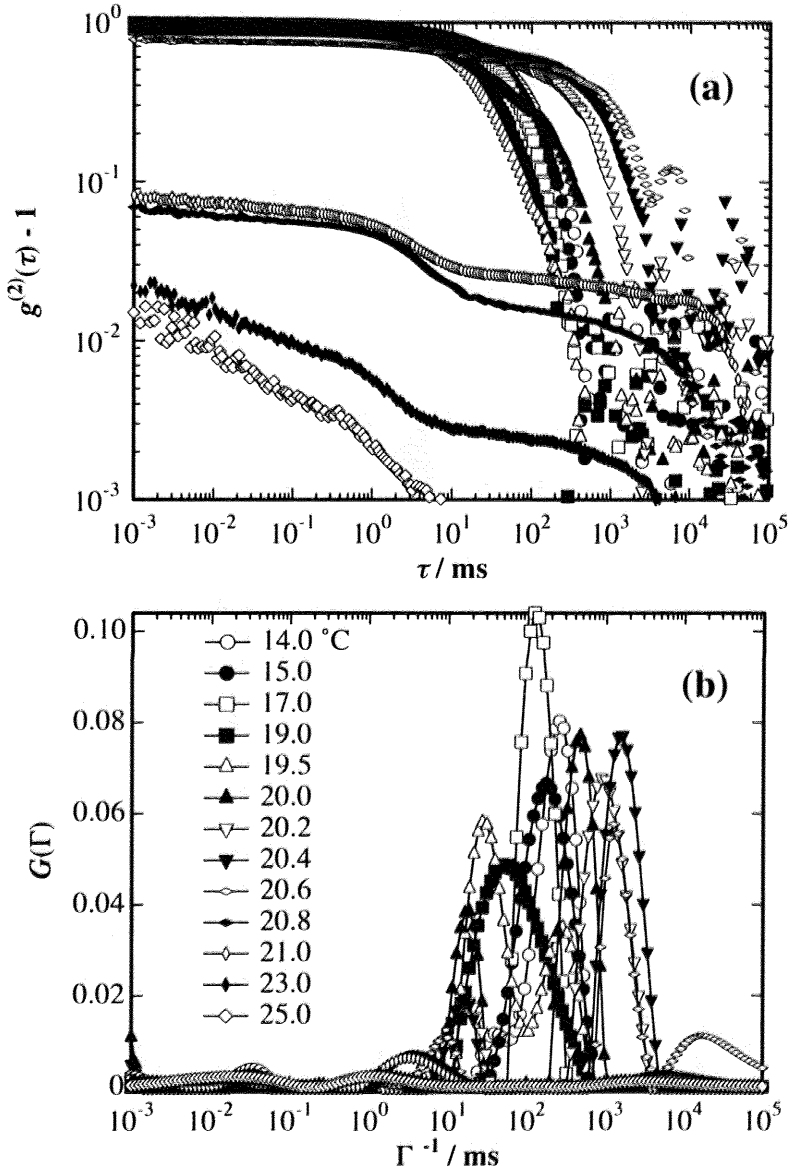


Figure 4.10: CFs of 17wt% EOVE-*b*-HOVE aqueous solution at various temperatures.

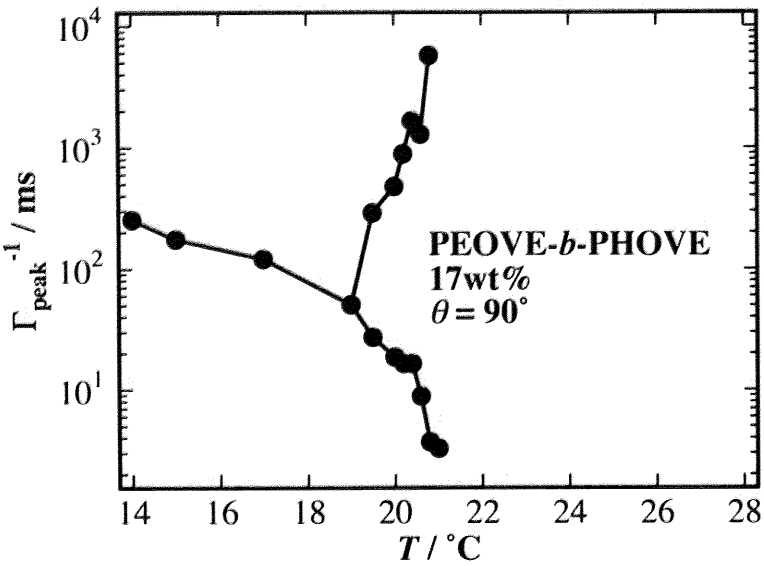


Figure 4.11: Variation of the characteristic decay time, $\Gamma_{\rm peak}^{-1}$, as a function of $T$. The $\Gamma_{\rm peak}^{-1}$ splits to two at 19 °C.

### 4.4.3 Nonergodic light scattering results

Figure 4.13 shows the light scattered intensity from the 17 wt% EOVE-*b*-HOVE aqueous solution. 100 sampling positions of a test tube were randomly chosen and a series of DLS measurements were carried out at various temperatures. At 15 °C, the intensity does not have noticeable position dependence. Therefore, one can call that this system is ergodic and $\langle I \rangle_{\rm T} = \langle I \rangle_{\rm E}$, where $\langle I \rangle_{\rm E}$ was obtained by averaging $\langle I \rangle_{\rm T}$ over 100 data points and is shown with the horizontal solid line. With increasing $T$, $\langle I \rangle_{\rm E}$ ($= \langle I \rangle_{\rm T}$) increased and reached a maximum at 19 °C. At 21.0 °C, there appeared strong position dependence in $\langle I \rangle_{\rm T}$, indicating that the system became nonergodic.

Figure 4.14 shows the temperature dependence of (a) $\langle I \rangle_{\rm E}$ and (b) the initial amplitude of the CFs, $g^{(2)}(\tau = 0) - 1$, for 17wt% EOVE-*b*-HOVE aqueous solution. At low $T$s, the scattered intensity was weak, implying that the system is a homogeneous polymer solution. With increasing temperature, on the other hand, the scattered intensity suddenly became strong at about 17 °C, which is identical to the temperature of the micelle formation determined by SANS experiment.[10] By further increasing temperature, the intensity slightly decreased and finally leveled off for $T > 20$ °C. Figure 4.14(b) shows that an ergodic-to-nonergodic transition took place at 20 °C. It

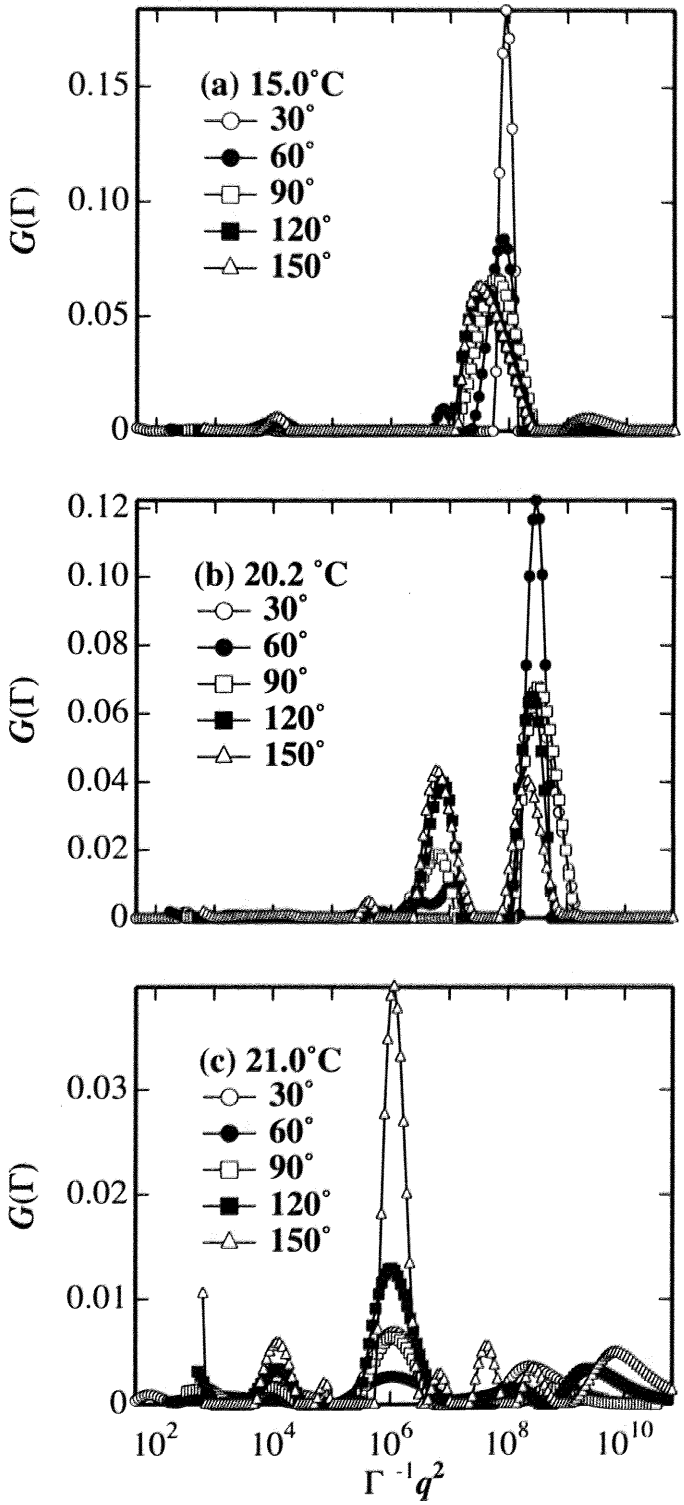


Figure 4.12: $G(\Gamma^{-1})$ vs $\Gamma^{-1}q^2$ plots of 17 wt% EOVE-*b*-HOVE aqueous solution at (a) 15.0 °C, (b) 20.2 °C, and (c) 21.0 °C.

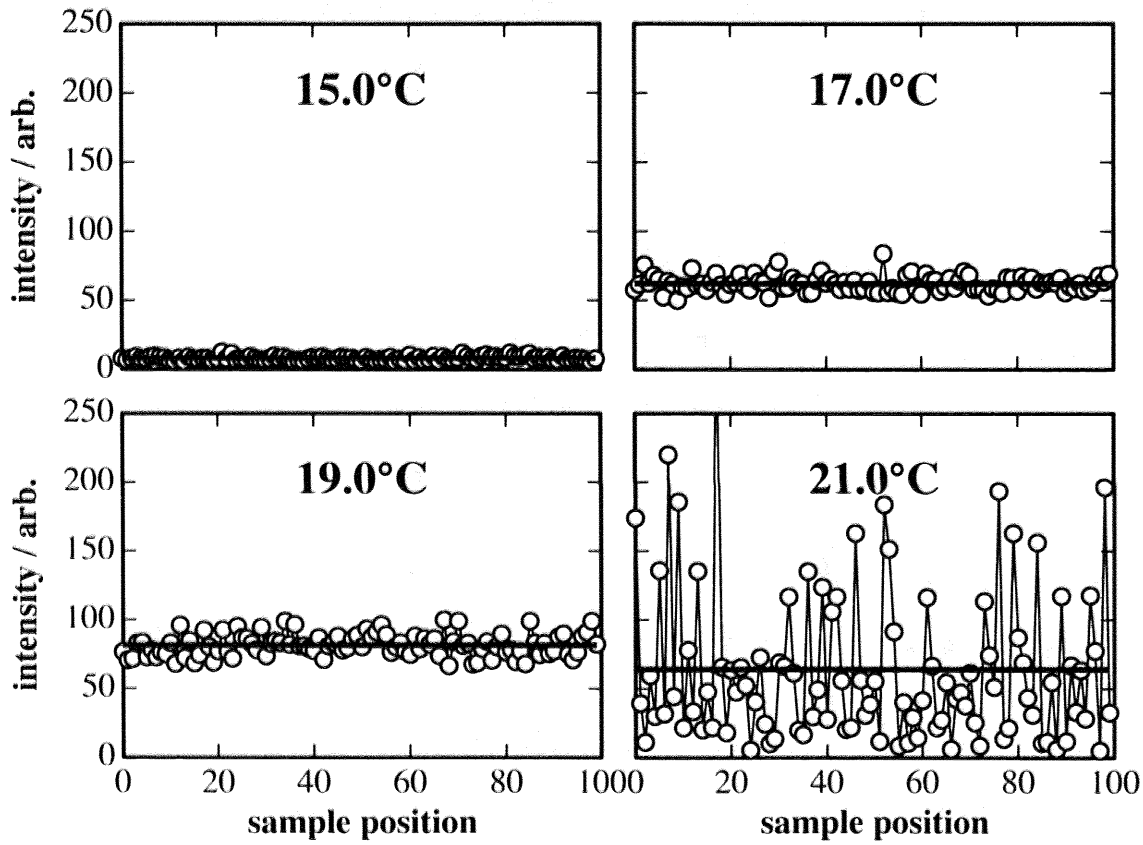


Figure 4.13: Speckle patterns at various temperatures.

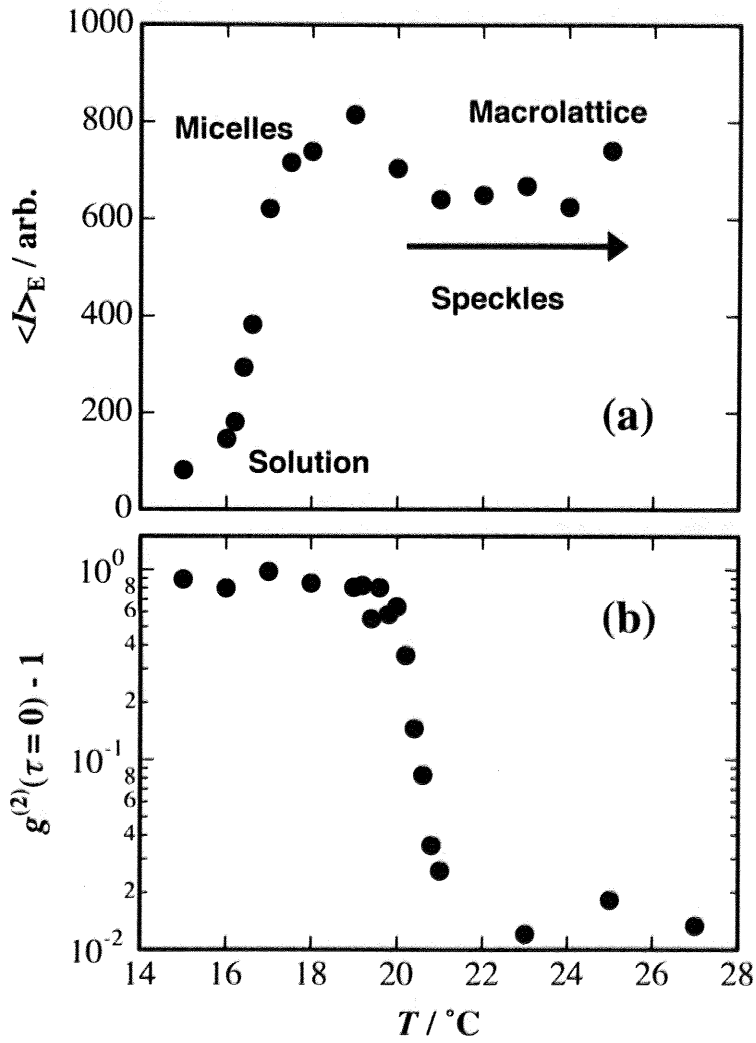


Figure 4.14: Temperature dependence of (a) $\langle I \rangle_E$ and (b) the initial amplitude of the CFs for 17 wt% EOVE-*b*-HOVE aqueous solution.

is worth noting that this temperature is not the same as the temperature at which $\langle I \rangle_E$ started to increase or reached a maximum. The ergodic-to-nonergodic transition corresponds to sol-gel transition, while the latter does to micelle formation. Hence, it can be concluded that DLS measurements are sensitive enough to discriminate the sol-gel transition from the micelle formation transition. Furthermore, these transitions have one-to-one correspondence to the rheological transitions. That is, micelle formation leads to Newtonian-to-non-Newtonian transition and sol-to-gel transition corresponds to non-Newtonian-to-plastic flow transition. Another interesting aspect which should be addressed here is that these transitions take place within a very narrow temperature window, i.e., 2 to 3 °C, which has not been observed in block copolymer-organic solvent systems.[22] Note that PEO-*b*-PPO-*b*-PEO (EO97-PO39-EO97) aqueous solutions requires about 20 °C temperature range (15 to 36.5 °C for this particular case) for these transitions, where the numbers indicate the numbers of monomeric unit in a block chain.[23] PS-*b*-PB block copolymers were also reported to have a wide temperature range of about 20 to 30 °C for these transitions.[15,16,24] The sharp structure transitions found in EOVE-*b*-HOVE is ascribed to strong temperature dependence of the interaction parameter of polyEOVE with water, of which origin has to been elucidated in more detail.

## 4.5 Structural transition of EOVE-*b*-HOVE in aqueous solutions

As discussed in the previous sections, EOVE-*b*-HOVE undergoes two transitions by increasing temperature. One is molecular dispersion-to-micelle transition and the other sol-to-gel transition. The latter transition was confirmed to be micelle-to-macrolattice transition by SANS. These transitions are schematically depicted in Figure 4.15(a to c). However, this is the case of concentrated solutions. In a dilute EOVE-*b*-HOVE solutions (e.g., 1 or 2 wt%) (Figure 4.15d), on the other hand, only polyEOVE chains coagulate and form a micellar structure (Figure 4.15f) with increasing temperature. Note here that this micelle formation proceeds via an intermediate state with extremely slow relaxation time. Though a direct observation on this intermediate state has not been carried out, an inter-connected chain cluster, depicted as Figure 4.15e, may be formed and this structure is responsible for a very slow

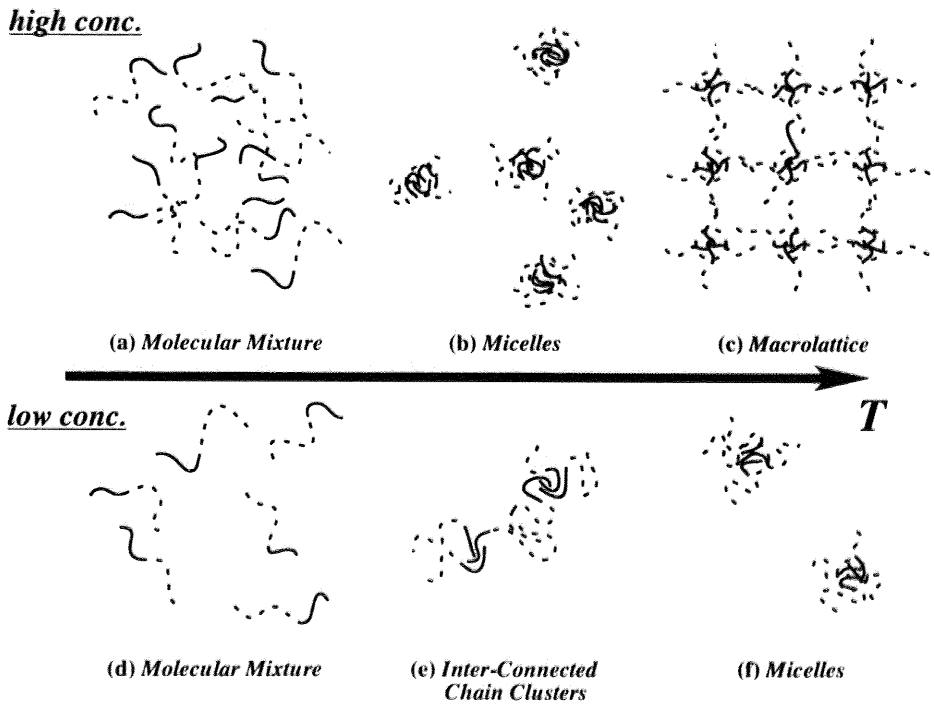


Figure 4.15: Schematic representation of showing two transitions from the molecular dispersion (a) to the crystal-like structure with macrolattice (c) by way of the micellar structure (b) in concentrated EOVE-*b*-HOVE aqueous solution. Figures (d) to (f) show the case of dilute EOVE-*b*-HOVE aqueous solution, where the intermediate state is deduced to be an inter-connected chain cluster structure.

relaxation observed for 1.0 wt% EOVE-*b*-HOVE aqueous solutions at $20 < T < 22$ ˚C.

## 4.6 Conclusion

DLS and rheological studies have been carried out on aqueous solutions of EOVE-*b*-HOVE, where polyEOVE is thermo-sensitive polymer and polyHOVE is hydrophilic polymer. DLS measurements for the corresponding homopolymer solutions suggested that the hydrodynamic radius of polyHOVE, $R_{\mathrm{H,HOVE}}$ is around 6 nm and is temperature independent. On the other hand, a strong clustering was observed for polyEOVE with increasing temperature. At low temperatures, the cluster size distribution function CDs showed two distinct peaks, corresponding to the fast (individual molecule) and slow modes (clusters). The value of $R_{\mathrm{H,fast}}$ was initially 3.7 nm at 12.6 ˚C, but due to clustering the relaxation mode corresponding to the individual molecules disappeared for $T > 17$ ˚C and gigantic clusters of the order of 200 nm are formed around LCST of polyEOVE, which finally precipitate. The DLS results for EOVE-*b*-HOVE aqueous solutions were similar to those of polyEOVE and exhibited a strong temperature dependence. Two-step structural transitions were observed, which are (I) molecular dispersion-to-micelles and (II) micelles-to-macrolattice transition. These behaviors are well correlated to the drastic changes in the rheological properties, i.e., Newtonian, non-Newtonian, and plastic flow. DLS measurements were successfully employed to discriminate these transitions as (I) a drastic increase in the scattered intensity and change in the hydrodynamic radius and (II) appearance of speckle pattern and suppression of the initial value of correlation functions. The temperature window required for these transitions were only a few degrees of Celsius, which is much narrower than those for block copolymers in organic solvent. This is one of the characteristic features of aqueous systems containing polyampholytes because of strong temperature dependence of hydrophobic interaction.

## References

[1] Chu, B. *Laser Light Scattering*, 2nd Ed. ed.; Academic Press, 1991.

[2] Siegert, A. F. J. *MIT Radiation Report* 1943, **465**.

[3] Schulz-DuBoir, E. O. In *Photon Correlation Techniques in Fulid Mechanics*; Schulz-DuBoir, E. O., Ed.; Springer-Verlag: Berlin, 1983; p15.

[4] Edwards, S.; Miller, A. G. *J. Phys. C: Solid State Phys.* 1976, **9**, 2011.

[5] Vink, H. *J. Chem. Soc., Faraday Trans.1* 1985, **81**, 1725.

[6] Pusey, P. N.; van Megen, W. *Physica A* 1989, **157**, 705.

[7] Joosten, J. G. H.; McCarthy, J. L.; Pusey, P. N. *Macromolecules* 1991, **24**, 6690.

[8] Shibayama, M. *Macromol. Chem. Phys.* 1998, **199**, 1.

[9] Furukawa, H.; Hirotsu, S. *J. Phys. Soc. Jpn.* 2002, **71**, 2873.

[10] Okabe, S.; Sugihara, S.; Aoshima, S.; Shibayama, M. *Macrmolecules* 2002, **35**, 8139.

[11] Aoshima, S.; Hashimoto, K. *J. Polym. Sci. PartA: Polym. Chem.* 2001, **39**, 746.

[12] Yang, H.; Hadziioannou, G.; Stein, R. S. *J. Polym. Sci., Polym. Phys. Ed.* 1983, **21**, 159.

[13] Yang, H.; Shibayama, M.; Stein, R. S.; Shimizu, N.; Hashimoto, T. *Macromolecules* 1986, **19**, 1667.

[14] Shibayama, M.; Tanaka, T.; Han, C. C. *J. Chem. Phys.* 1992, **97**, 6829.

[15] Watanabe, H.; Kotaka, T.; Hashimoto, T.; Shibayama, M.; Kawai, H. *J. Rheology* 1982, **26**, 153.

[16] Hashimoto, T.; Shibayama, M.; Kawai, H.; Watanabe, H.; Kotaka, T. *Macomolecules* 1983, **16**, 361.

[17] Winter, H. H.; Chambon, F. *J. Rheology* 1986, **30**, 367.

[18] Winter, H. H.; Mours, M. *Adv. Polym. Sci.* 1997, **134**, 167.

[19] Peters, R. In *Dynamic Light Scattering: The Methods and Some Applications*; Brown, W. Ed.; Oxford Univ. Press: Oxford, U.K., 1993.

[20] Provencher, S.W.; Stepanek, P. *Part. Part. Syst. Charact.* 1996, **13**, 291.

[21] Tanaka, T. In *Dynamic Light Scattering*; Pecora, R., Ed.; Plenum Publishing: New York, 1985; pp347 - 362.

[22] Hamley, I. W. *The Physics of Block Copolymers*; Oxford University Press: Oxford, 1998.

[23] Mortensen, K. *Progress in Colloid and Polym. Sci.* 1993, **91**, 69.

[24] Shibayama, M.; Hashimoto, T.; Kawai, H. *Macomolecules* 1983, **16**, 16.

# Chapter 5

# Water-induced Self-assembling of Solvent-sensitive Block Copolymer

## 5.1 Introduction

Among various combinations of block chains, it was found that poly(2-phenoxyethyl vinyl ether)-*block*-poly(2-methoxyethyl vinyl ether) (PhOVE-*b*-MOVE) is very sensitive to the choice of solvents.[1] The chemical structure of PhOVE-*b*-MOVE is shown in Figure 5.1. This is due to the difference in solubility of the constituent homopolymers, polyPhOVE and polyMOVE, to solvents as shown in Table 8.1. The circles and crosses in Table 8.1 respectively mean that the polymers are soluble and insoluble to the solvents at room temperature. polyPhOVE is soluble to non-polar solvents while polyMOVE to polar solvents, indicating that they have hydrophobic and hydrophilic nature, respectively. As a result, PhOVE-*b*-MOVE behaves as a polyampholyte, like a "polymer soap".

In this chapter, acetone and water were chosen as a common and a selective sol-

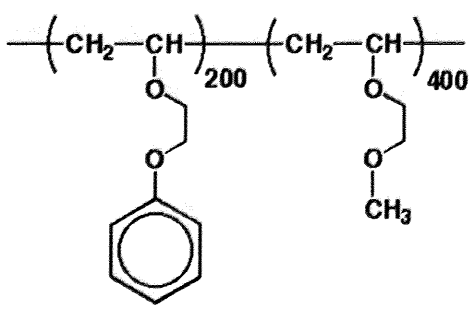


Figure 5.1: Chemical structure of PhOVE-*b*-MOVE.

Table 5.1: Solubility characteristics of polyPhOVE and polyMOVE at room temperature. ○: soluble, ×: insoluble.

| solvent | polyPhOVE | polyMOVE |
|---|---|---|
| water | × | ○ |
| methanol | × | ○ |
| ethanol | × | ○ |
| *n*-hexane | × | × |
| heptane | × | × |
| cyclohexane | × | ○ |
| toluene | ○ | ○ |
| acetone | ○ | ○ |

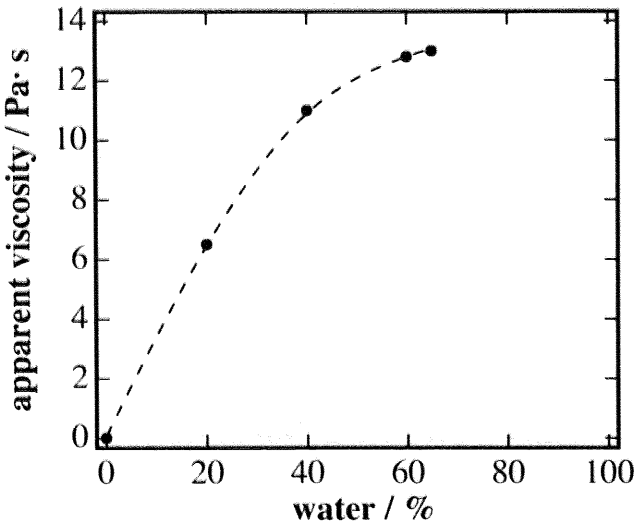


Figure 5.2: Apparent viscosity (shear rate = 10 $s^{-1}$) of PhOVE-*b*-MOVE gels with different solvent compositions (acetone/water).

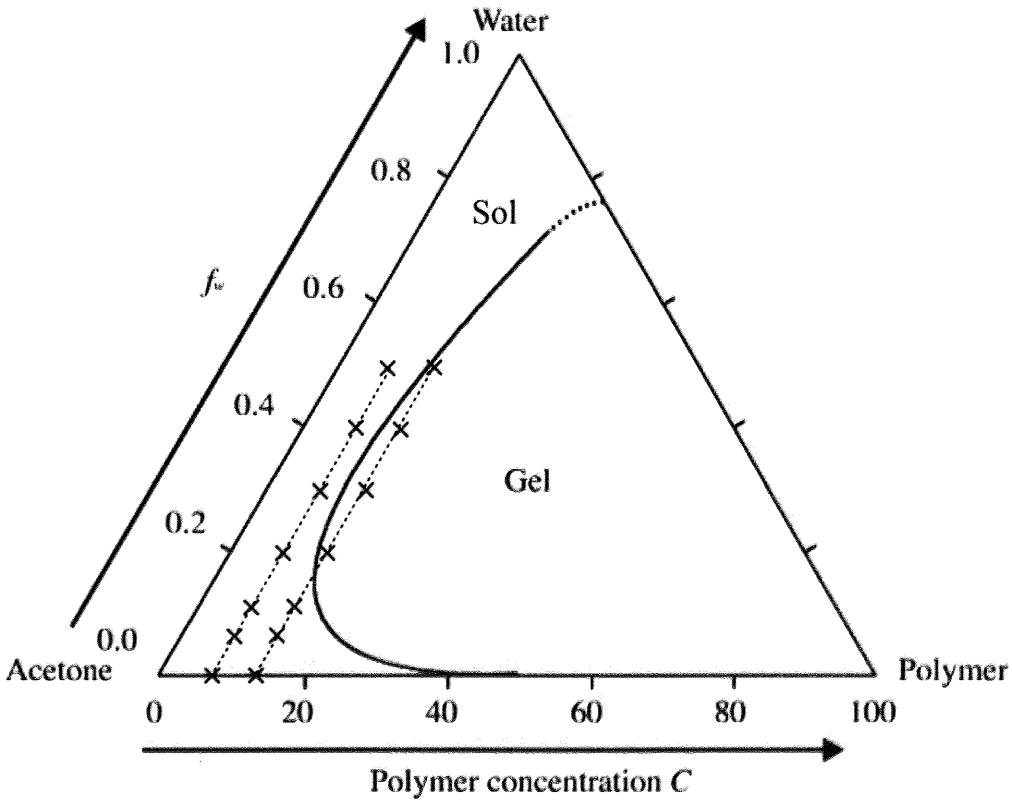


Figure 5.3: Triangle phase diagram for PhOVE-*b*-MOVE/acetone/water at 30 ℃.

vent, respectively. Interestingly enough, it was revealed that the viscosity of PhOVE-*b*-MOVE acetone solutions increased abruptly but continuously by adding water (Figure 5.2). In addition, the system underwent a sol-gel transition by addition of water, where the gel phase was determined by tilting-a-tube method. Figure 5.3 shows a triangle phase diagram of the PhOVE-*b*-MOVE/acetone/water solutions at 30 °C. The horizontal axis is the polymer concentration, C, and the other axis is the solvent composition, $f_w$. Here we define the value $C$ and $f_w$ as the weight percentage of the polymer in solution and the weight fraction of water in the mixed acetone/water solvent, respectively. The phase diagram is divided to two regions, i.e., solution and gel. In this chapter, SANS investigations are carried out on the microphase structures of PhOVE-*b*-MOVE solutions and gels in various solvent compositions and polymer concentrations.

## 5.2 Experimental Section

### 5.2.1 Samples

PhOVE-*b*-MOVE with a narrow molecular weight distribution ($\bar{M}_n$ = 73.7 × $10^3$, $\bar{M}_w/\bar{M}_n$ = 1.18) was synthesized by living cationic polymerization consisting of 200 and 400 monomer units for polyPhOVE and polyMOVE, respectively.[1] The number average molecular weights, $M_n$, of polyPhOVE and polyMOVE are 32.8 × $10^3$ and 40.9 × $10^3$, respectively. Hence, the molecular weight ratio of polyPhOVE to the total block copolymer is 0.445. The corresponding homopolymer polyPhOVE was polymerized in toluene at 0 °C in the presence of ethyl acetate with $Et_{1.5}AlCl_{1.5}$ under dried nitrogen atmosphere. Without an induction phase, the polymerization proceeded smoothly to reach 100 % conversion and a monotonous increase in number average molecular weight with monomer conversion was observed, indicating living polymerization. After finishing the polymerization of PhOVE (20.5 hr), the second monomer, MOVE in neat, was added into the system. The sequential living cationic copolymerization, after sufficient conversion time, namely 3.0 hr (total 23.5 hr), was quenched with methanol containing a small amount of aqueous ammonia solution (0.3 wt%) and washed with 0.6-N hydrochloric acid to remove the initiator residues and to neutralize the system. The synthesized PhOVE-*b*-MOVE was collected by evaporation of the solvents under reduced pressure.

Gel and solution samples of PhOVE-*b*-MOVE were prepared by first dissolving the polymer into acetone and then adding water to make series of samples with the same polymer concentration but with different water contents. Before and after adding water, all the samples were shaken for 30 minutes for complete dissolution. For $C = 12$ wt% samples, the samples were heated with a water bath at 45 °C after adding water to avoid non-uniform solvation. For all the SANS experiments except for the contrast variation experiment, deuterated acetone (99.9 % deuteration) and deuterium oxide (99.9 % deuteration) were used as the solvents in order to obtain enough scattering contrast between the polymer and the solvents.

### 5.2.2 SANS

All the SANS data in this chapter were acquired using SANS-U. The incident neutron wavelength was 0.70 nm with a 10 % distribution. The temperature of the samples was controlled with a water-circulating bath (NESLAB RTE-111M) with the precision of ±0.1 °C. Samples in quartz cells of 2 or 4 mm thickness were measured for sufficient period of time depending on the transmission and the scattering power of the samples to gain enough statistics, namely 10 to 120 minutes. The sample-to-detector distances were 2 and 8 m. The scattering intensities were circularly averaged and corrected for transmission, cell scattering, and incoherent backgrounds, and then were combined to a master scattering function to cover a wide range of the scattering vector, $q$, i.e., $0.06 \leq q \leq 1.5$ nm$^{-1}$. Thus corrected scattering intensity was scaled to the absolute scattering intensity, $I(q)$, with the incoherent scattering intensity from a Lupolen secondary standard sample.

## 5.3 Results and Discussion

### 5.3.1 Acetone solutions

In acetone solutions, the scattering intensity functions, $I(q)$s, were relatively low and was a monotonous decreasing function with $q$. According to the following equation,[2] the correlation length, $\xi$, was evaluated.

$$I_{\mathrm{OZ}}(q) = \frac{I_{\mathrm{OZ}}(q=0)}{1+\xi^2 q^2} \tag{5.1}$$

Figure 5.4 shows Ornstein-Zernike (OZ) plots ($I^{-1}(q)$ vs $q^2$) of the PhOVE-*b*-MOVE

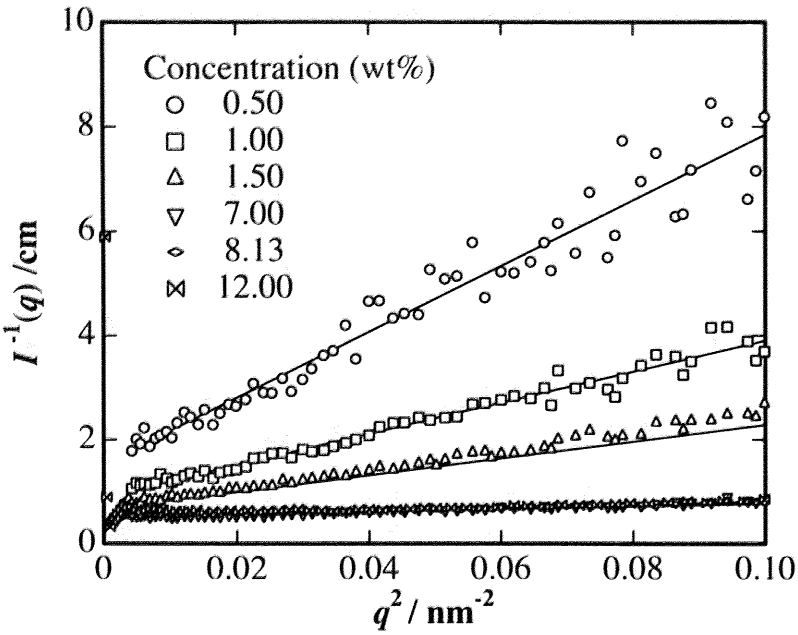


Figure 5.4: Ornstein-Zernike plots of PhOVE-*b*-MOVE in d-acetone solutions observed at 20 °C.

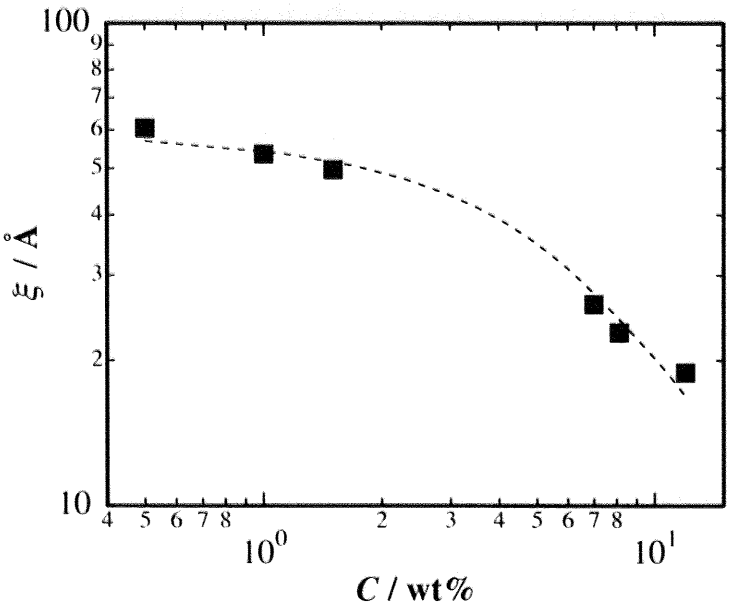


Figure 5.5: Variation of $\xi$ with $C$ for PhOVE-*b*-MOVE acetone solutions observed at 20 °C.

in deuterated acetone (d-acetone) solutions in the concentration regimes of $C = 0.5$ wt% to 12 wt%. The SANS data seem to be well fitted to OZ functions. Figure 5.5 shows the variation of $\xi$ with $C$. The dashed line is guide for the eye. For $C \geq 7$ wt%, the following relation was obtained $\xi \sim C^{-0.58}$. Hence, it is deduced that the PhOVE-*b*-MOVE polymer chains are somewhat in expanded state as in a good solvent and chain overlapping takes place for at least $C \geq 7$ wt%.

### 5.3.2 Microphase separation accompanying sol-gel transition

In Figure 5.6 is shown the scattering intensity profiles, $I(q)$s, for PhOVE-*b*-MOVE solutions at (a) $C = 7$ wt% and (b) $C = 12$ wt%, with different solvent compositions, fws. In the case of acetone solution, i.e., $f_w = 0$, $I(q)$ is well described by eq. 5.1 as discussed above. However, by addition of small amount of water, e.g., $f_w = 0.05$, a broad peak appeared at $q \approx 0.12$ nm$^{-1}$ for $C = 7$ wt% and at $q \approx 0.15$ nm$^{-1}$ for $C = 12$ wt%. The peaks evolved with increasing water content and then new peaks appeared at a lower $q$ region as shown by the thick arrows. As a result, $I(q)$ increased dramatically by hundred times in the intensity with distinct peaks in the lower $q$ region. All of these peaks are more clearly seen in the samples of $C = 12$ wt%, where multiple peaks at low $q$'s indicate the presence of well-ordered structure as will be discussed later.

These peaks in Figure 5.6 suggest emergence of a nano-order assembled structure in the polymer solution. The peaks of $I(q)$s at higher $q$ values ($q > 0.3$ nm$^{-1}$) shown by the thin arrows indicate the existence of spherical domains. On the other hand, the peaks at lower $q$ value ($q < 0.3$ nm$^{-1}$) shown by thick arrows indicate a highly ordered arrangement of the domains. From the relative positions of the 1st, 2nd, and 3rd peaks of $C = 12$ wt%, i.e., $1, \sqrt{2}, \sqrt{3}$, we can assign this ordered structure to be a body-centered cubic (bcc). It should be also noted here that the appearance of these peaks is very different from the case of heat-induced microphase separation shown in Chapter 3,[3] where the peaks related to spherical micelles appear first followed by emergence of interference peaks. In the next section, fitting analyses are carried out for these profiles.

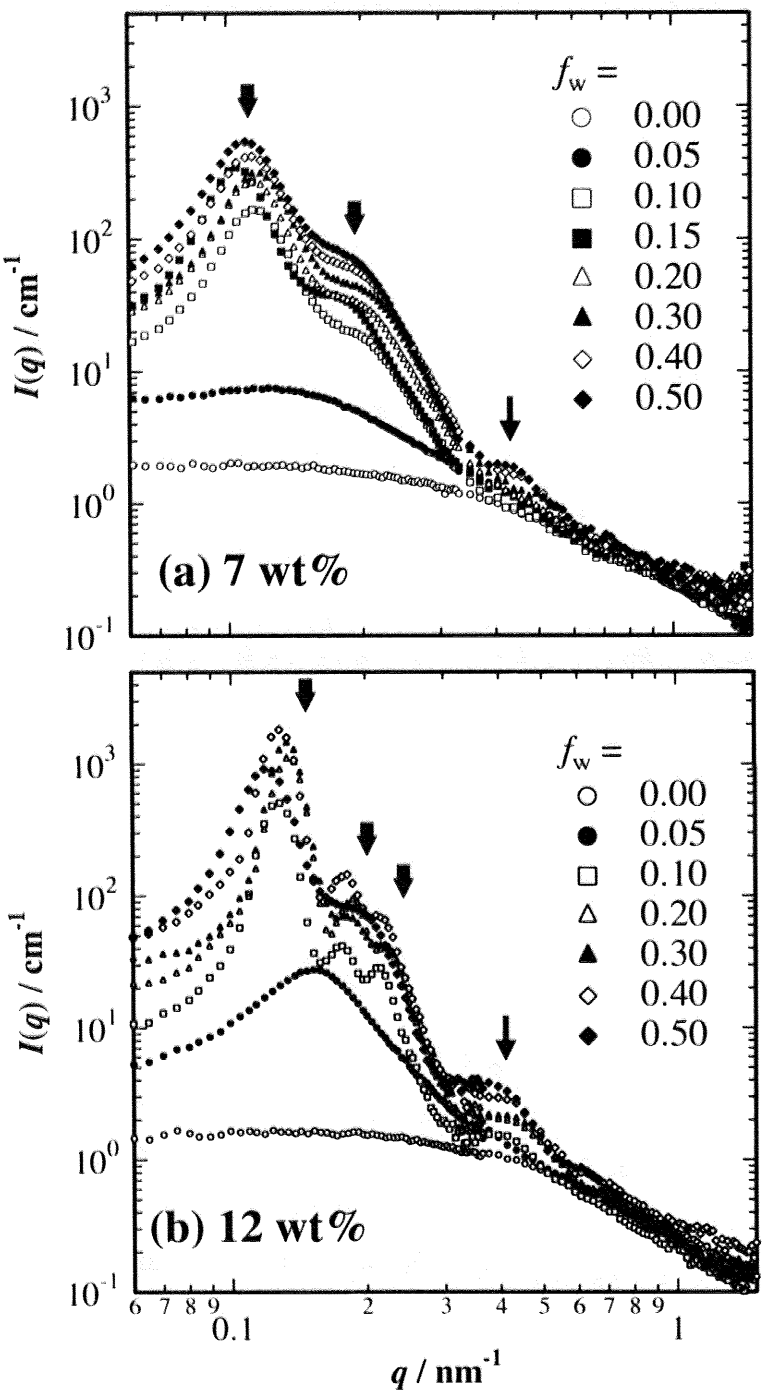


Figure 5.6: Scattering intensity functions, $I(q)$s, for (a) 7 and (b) 12 wt% PhOVE-*b*-MOVE in acetone/water with different water weight fractions, $f_w$s.

### 5.3.3 Quantitative analysis of the microphase separated structure

In order to quantify the structure, curve fitting was performed for the SANS profiles using the three dimensional paracrystal theory as was introduced in Chapter 3. The scattering function consists of two parts, namely the form factor for non-interfering spherical particles, $P(q)$, and the lattice factor, $Z(q)$. However the profiles did not follow Porod's rule in higher $q$ region ($q \geq 0.5$ nm$^{-1}$), and $I(q)$ decreased with a power of -2 instead of -4. This $q$-dependence of $I(q)$ indicates that the spherical domains are embedded in a semi-dilute polymer solution. The fitting function is then reconstructed by considering the contribution from scattering of the matrix and it is expressed as:

$$I(q) = I_{\text{particle}}(q) + I_{\text{OZ}}(q) \tag{5.2}$$

$$I_{\text{particle}}(q) = P(q)Z(q) \tag{5.3}$$

where the first and second terms of the RHS represent the scattered intensities for spherical domains with the particle factor P(q) and lattice factor Z(q) and for semi-dilute solutions, i.e., the OZ function (eq. 5.1), respectively. Note that this assumption neglects the detailed conformation of polymer chains near the micelle core-corona interface, which still nicely reproduces the microphase separated structure of block copolymer solutions.[4]

In Figure 5.7 is shown an example of the results of curve fitting for $f_w = 0.1$. The fitted curve designated by the solid line reproduced the observed scattering function quite well. The two-dot-chain line indicates the contribution of $I_{\text{matrix}}(q)$, from which the correlation length, $\xi$, was evaluated to be 1.9 nm. This value is in good agreement with that observed in 12 wt% acetone solution of PhOVE-*b*-MOVE. Hence, the model, spherical domains embedded in a polymer solution, seems to be valid. From the fitting for $q \leq 0.5$ nm$^{-1}$, the structure parameters, i.e., the size of the microdomains and the lattice spacing, $R$ and $a$, their relative deviations, $\Delta R/R$ and $\Delta a/a$, were obtained. The same fitting was carried out for the other profiles showing distinct peaks. The variations of these structure parameters with fw are shown in Figure 5.8. As shown in the figure, the radius of the spherical domains, $R$, seems to be an increasing function of $f_w$, while that of $C = 7$ wt% is somewhat scattered. The larger in $C$, the larger in $R$. This is due to an increase in the Flory interaction

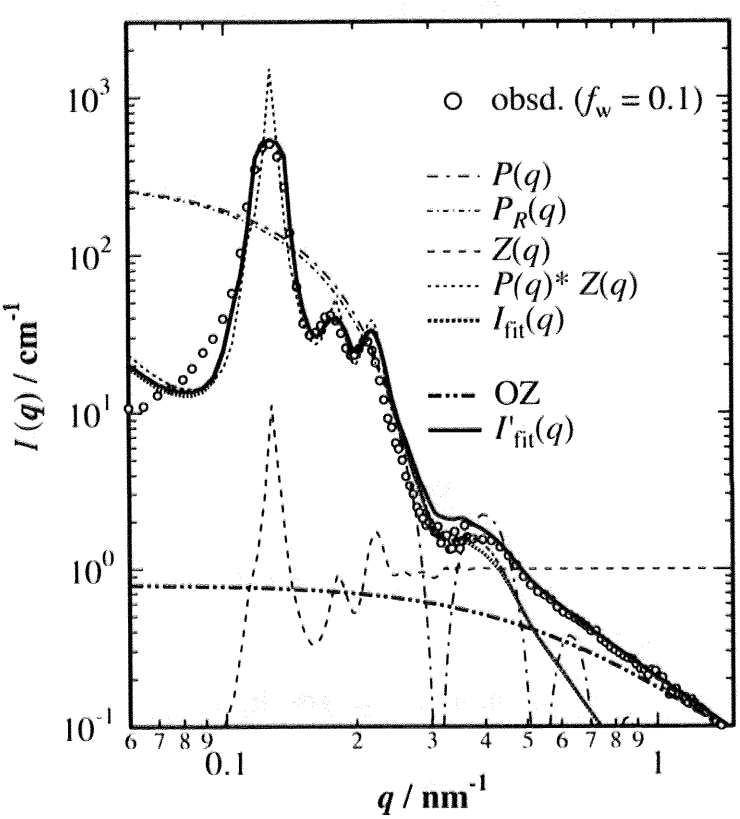


Figure 5.7: Result of curve fitting of $I(q)$ for microphase-separated PhOVE-*b*-MOVE for C = 12 wt% and $f_w = 0.1$.

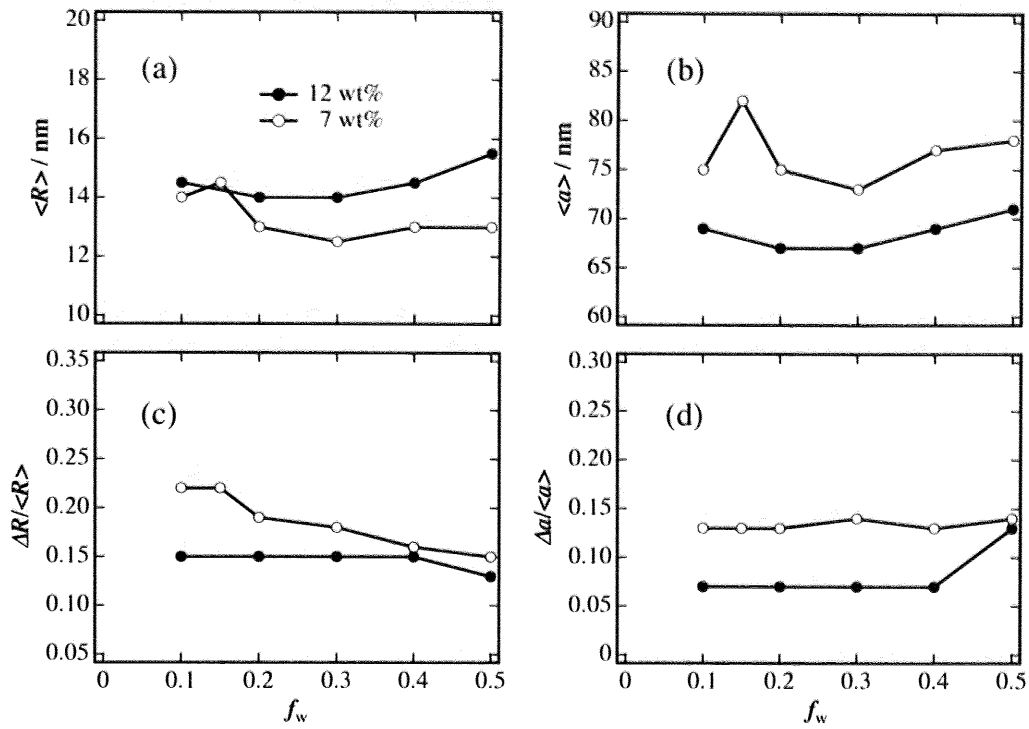


Figure 5.8: Variations of the structure parameters, (a) $R$, (b) $a$, (c) $\Delta R/R$, and (d) $\Delta a/a$, evaluated by curve fitting.

parameter, $\chi$, by increasing $C$ or $f_w$. The radius of spherical micro-domains in a good solvent is an increasing function of $\chi$ as discussed elsewhere.[5] The lattice size, $a$, also tends to increase with increase in $f_w$, and $a = 79.0$ and 65.0 nm in average for $C = 7$ wt% and 12 wt%, respectively. Thermodynamically, the value of $a$ is determined by minimizing density fluctuations of the solution/gels in the presence of dispersing domains. As $C$ increases, $R$ increases and $a$ decreases as in the case of other block copolymers in selective solvents.[6] The variations of (c) $\Delta R/R$ and (d) $\Delta a/a$ were also evaluated owing to the curve fitting. The value of $\Delta R/R$ is, in general, decreasing functions with increase in $f_w$ and $C$, suggesting more uniform spherical domain due to stronger segregation of the two constituting chains. Likewise, the value of $\Delta a/a$ decreased with increasing $C$.

We can attribute this variation to the variation of the number of formed domains per unit volume, $n$. As a bcc lattice consists of two spheres in one unit cell, $n$, is given from $a$ by using the following relationship,

$$n = \frac{2}{a^3} \tag{5.4}$$

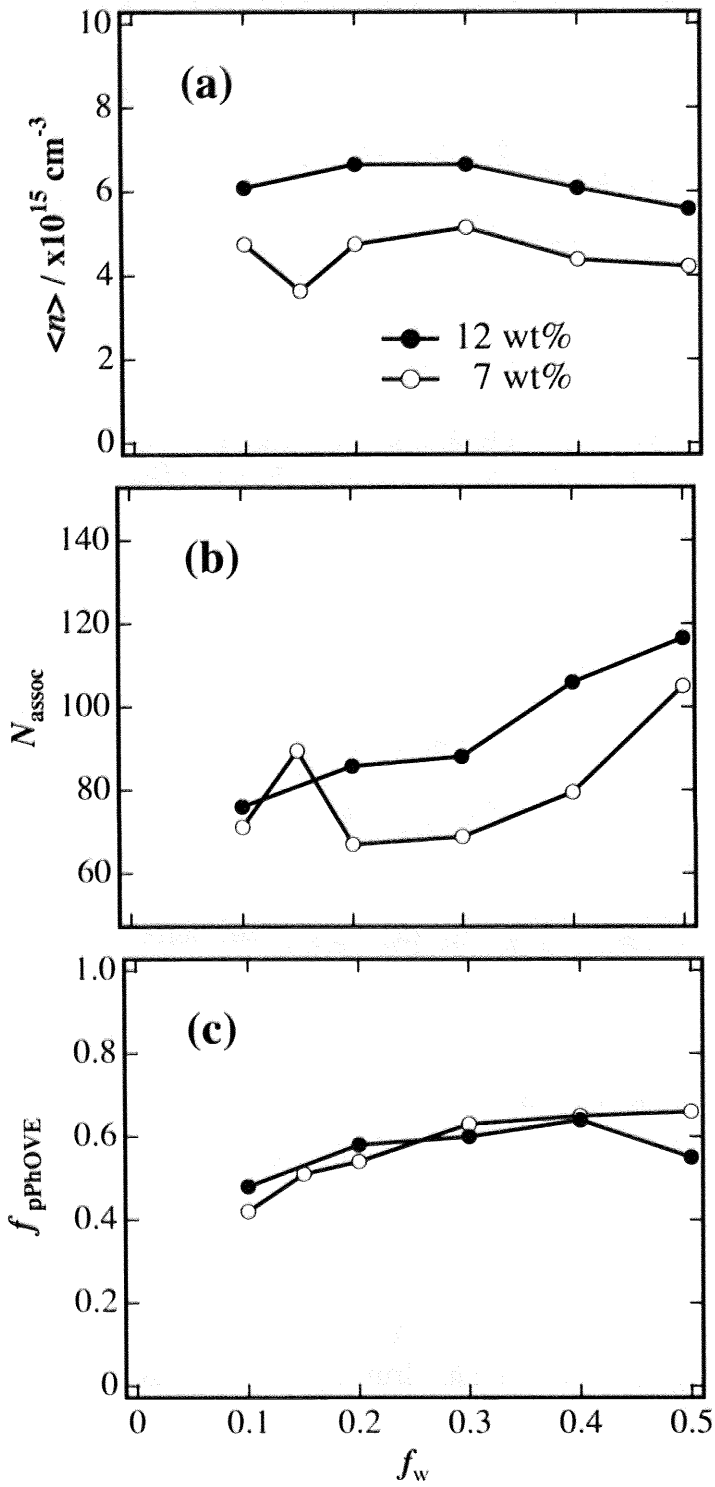


Figure 5.9: Variations of the structure parameters, (a) $n$, (b) $N_{\mathrm{assoc}}$, and (c) $f_{\mathrm{polyPhOVE}}$.

$$a = \sqrt{2}\frac{2\pi}{q_{\max}} \tag{5.5}$$

Here, $q_{\max}$ is the first peak position of the SANS profile, which comes from the (110) reflection of the bcc lattice. Thus obtained value of $n$ is plotted in Figure 5.9(a) as a function of $f_w$. Interestingly, $n$ is rather invariant irrespective of $f_w$. This means that the number of domains is pre-determined when the polymer concentration is fixed. The association number, i.e., the number of polymer chains per spherical domain, $N_{\text{assoc}}$ can be evaluated via the following equation,

$$N_{\text{assoc}} = \frac{f_{\text{polyPhOVE}} V_{\text{domain}} d_{\text{domain}}}{M_{\text{polyPhOVE}}} N_A \tag{5.6}$$

where $V_{\text{domain}}$, $M_{\text{polyPhOVE}}$, and $d_{\text{domain}}$ are the volume fraction of polyPhOVE, the volume of the spherical domain, the molecular weight of polyPhOVE and the mass density of the spherical domain, respectively, and $N_A$ is the Avogadro's number. Here, let us assume $d_{\text{domain}} = 1.0$ g/cm$^3$ for simplicity. The symbol, $f_{\text{polyPhOVE}}$, is the polyPhOVE volume fraction in the spherical domain given by

$$f_{\text{polyPhOVE}} = \frac{(\rho - \rho_{\text{solv}}) f_{\text{polyMOVE}} - \sqrt{\dfrac{I(0)_{\text{obs}} a^3}{2V_{\text{domain}}^2}}}{\rho_{\text{polyPhOVE}} - \rho_{\text{solv}}} \tag{5.7}$$

Figure 5.9(b) and (c) show the variations of $N_{\text{assoc}}$ and $f_{\text{polyPhOVE}}$ with $f_w$ for the cases of 7 and 12 wt%. $N_{\text{assoc}}$ increases with $f_w$ because $f_{\text{polyPhOVE}}$ increases with $f_w$ as shown in Fig. 5.9c. The increase of $f_{\text{polyPhOVE}}$ with $f_w$ is due to the fact that the initial polymer concentrationin acetone, $C_0$, was different. The higher the $f_w$, the higher $C_0$, resulting in an association with a larger number of polymer chains after water addition. Then, the solvent in the polyPhOVE domains is squeezed out by increasing $f_w$ by keeping $N_{\text{assoc}}$ determined at the onset of phase separation.

As mentioned above, it was shown that the polymer chains are assembled into spherical microdomains packed in a bcc style after addition of moderate amount of water. This formation of microphase-separated structure is the origin of the phenomenological sol-gel transition shown in Figure 5.3. In the next section, let us examine the architecture of the microphase separation.

### 5.3.4 Architecture of the microphase separation in gel state

Let us first propose two models for the spatial variations in scattering length density as shown in Figure 5.10. The model (a) is a spherical domain structure with

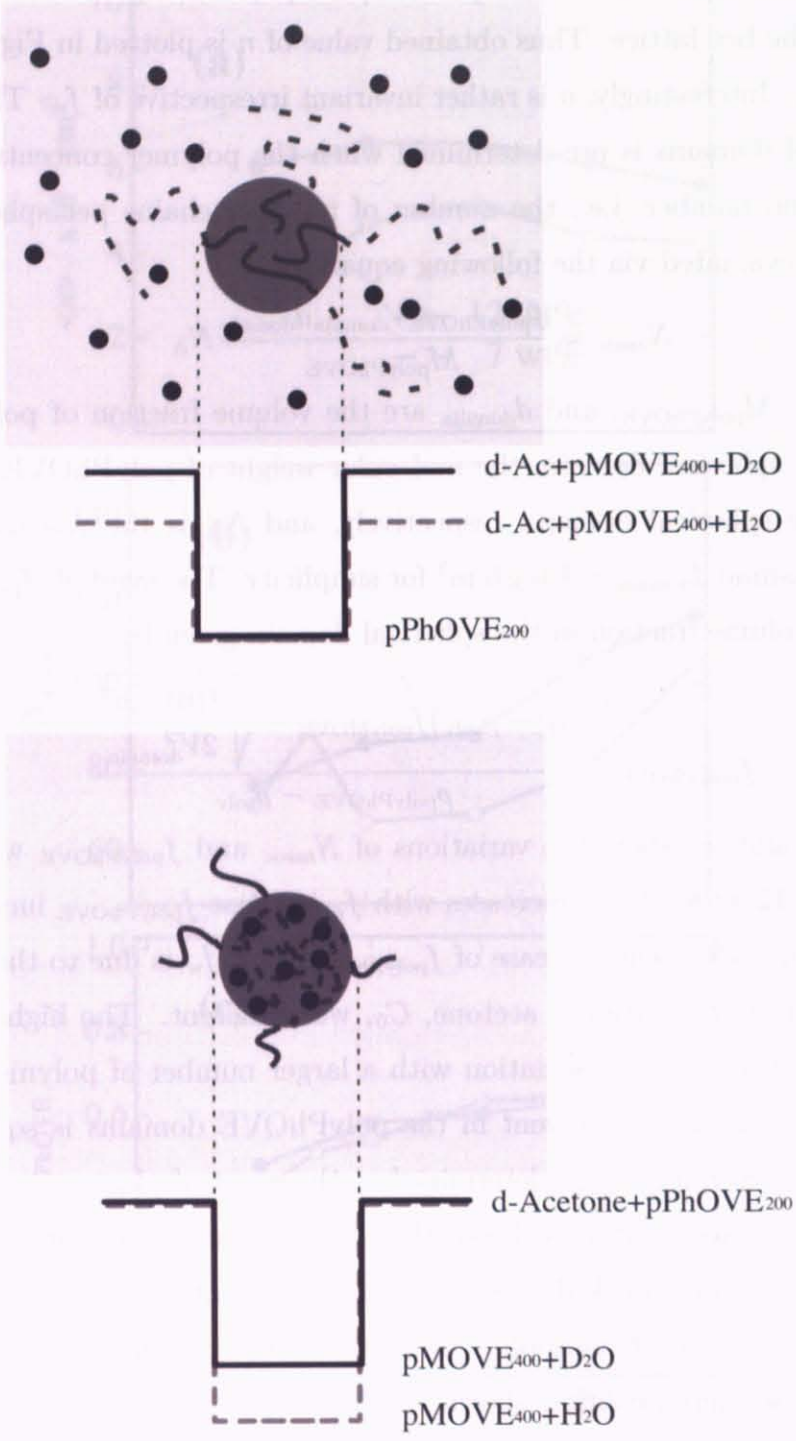


Figure 5.10: Models and the scattering-length density profiles of a PhOVE-*b*-MOVE spherical domain.

polyPhOVE, and the model (b) is *vice versa* with polyMOVE. In the case of model (a), added water molecules are dispersed into acetone matrix and the solvent becomes poorer. This results in formation of hydrophobic polyPhOVE domain by excluding polyMOVE chains and the solvent. In the model (b), on the other hand, the added water molecules are trapped into the domain with rather hydrophilic polyMOVE chains to prevent the unfavorable water-polyPhOVE interaction. These two models were examined by using a contrast variation method. As is given by eqs. 5.3 and 3.3, $I(q)$ is proportional to the square of the scattering length densities between the particles and the matrix:

$$I(q)_{\mathrm{obs}} \sim \Delta\rho^2 = (\rho_{\mathrm{matrix}} - \rho_{\mathrm{core}})^2 \tag{5.8}$$

In this experiment, $H_2O$ was employed instead of $D_2O$ as an adding solvent to change the contrast of $\rho$ between the matrix and the domain to trace the water molecules after the addition. As the value of $\rho$ for $H_2O$ is negative and those of the others are all positive, $H_2O$ acts to lower the $\rho$ value of its surroundings. The ratio of the scattering intensities between the H and D systems is given by

$$\frac{I(q)_{\mathrm{H}}}{I(q)_{\mathrm{D}}} = \frac{([(\rho_{\mathrm{polyMOVE}} - \rho_{\mathrm{solv,H}})f_{\mathrm{polyMOVE}} - (\rho_{\mathrm{polyPhOVE}} - \rho_{\mathrm{solv,H}})f_{\mathrm{polyPhOVE}}])^2}{([(\rho_{\mathrm{polyMOVE}} - \rho_{\mathrm{solv,D}})f_{\mathrm{polyMOVE}} - (\rho_{\mathrm{polyPhOVE}} - \rho_{\mathrm{solv,D}})f_{\mathrm{polyPhOVE}}])^2} \tag{5.9}$$

where $\rho_{\mathrm{i}}$ and $f_{\mathrm{i}}$ are the scattering length density and the volume fraction of i (= polyPhOVE or polyMOVE) in the respective domain/matrix. The calculated $\rho$ values of polymer chains and mixed D/H-solvents of $f_{\mathrm{w}} = 0.1$ are as follows: $\rho_{\mathrm{polyMOVE}} = 0.439 \times 10^{10}$, $\rho_{\mathrm{polyPhOVE}} = 1.217 \times 10^{10}$, $\rho_{\mathrm{solv,H}} = 4.86 \times 10^{10}$, and $\rho_{\mathrm{solv,D}} = 5.54 \times 10^{10}$ $\mathrm{cm}^{-2}$. In the case of $C = 7$ wt%, the values of $f_{\mathrm{polyMOVE}} = 0.036$ and $f_{\mathrm{polyPhOVE}} = 0.42$ and the ratio of $I(q)$s was evaluated to be 0.7. In Figure 5.11 is shown the result of the experiment in the sample of $C = 7$ wt% with $f_{\mathrm{w}} = 0.1$. The calculated $I(q)$ was almost superimposed only by multiplying $I(q)$ with the ratio calculated with eq. 5.9, showing a good agreement with the experimental result. As shown in the figure, a similar shape profile with a decrease in the scattering intensity was obtained. This means that the shapes of the formed microphase structures are the same and only the difference in $\rho_{\mathrm{matrix}}$ and $\rho_{\mathrm{core}}$ has been changed by H/D substitution. Considering the decrease in the intensity, we can conclude that the domains are formed by polyPhOVE chains as shown in Figure 5.10(a).

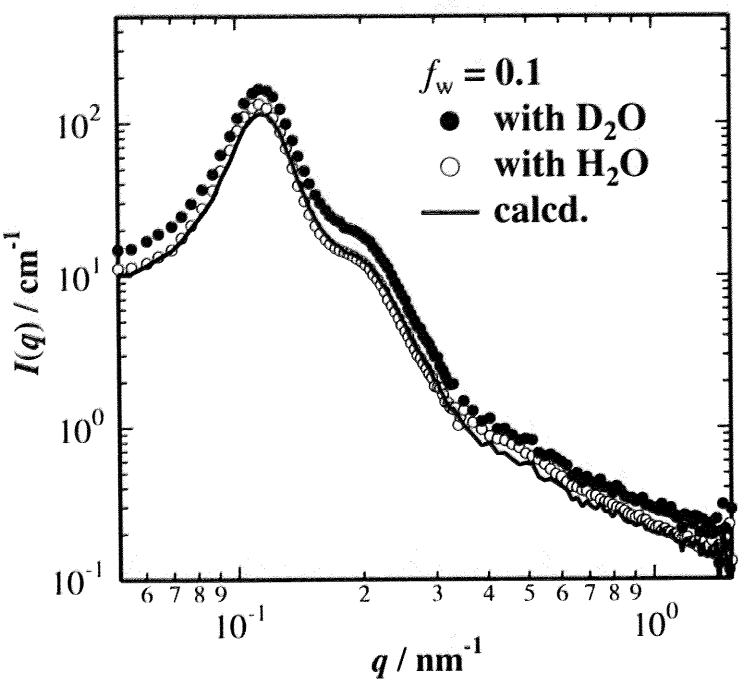


Figure 5.11: SANS results of the contrast variation experiment for PhOVE-*b*-MOVE acetone/water solution with $C = 7$ wt% and $f_w = 0.1$.

### 5.3.5 Comparison of the heat-induced and the water-induced microphase separation

In chapter 3, we discussed a heat-induced phase separation in poly(2-ethoxyethyl vinyl ether)-*block*-poly(2-hydroxyethyl vinyl ether) (EOVE-*b*-HOVE) aqueous solutions. In the case of EOVE-*b*-HOVE, a micelle formation undergoes first, followed by rearrangement to a bcc packed structure. For comparison, the phase separation behavior of poly(2-ethoxyethyl vinyl ether)-*block*-poly(2-methoxyethyl vinyl ether) (EOVE-*b*-MOVE) aqueous solutions was studied and it was found that this system also undergoes a heat-induced phase separation. In both cases, polyEOVE becomes non-soluble to water above 20 °C. The difference between the water-induced phase separation studied here in PhOVE-*b*-MOVE/acetone/water and the heat-induced phase separation observed in EOVE-*b*-MOVE and EOVE-*b*-HOVE are due to the nature of environmental-sensitivity of the polyPhOVE (non-soluble group to water) and polyEOVE (temperature-sensitive). Interestingly enough, it was found that the evolutions of microphase separation are different between the two systems.

In Figure 5.12 is shown series of SANS profiles for (a) 20 wt% EOVE-*b*-MOVE aq.

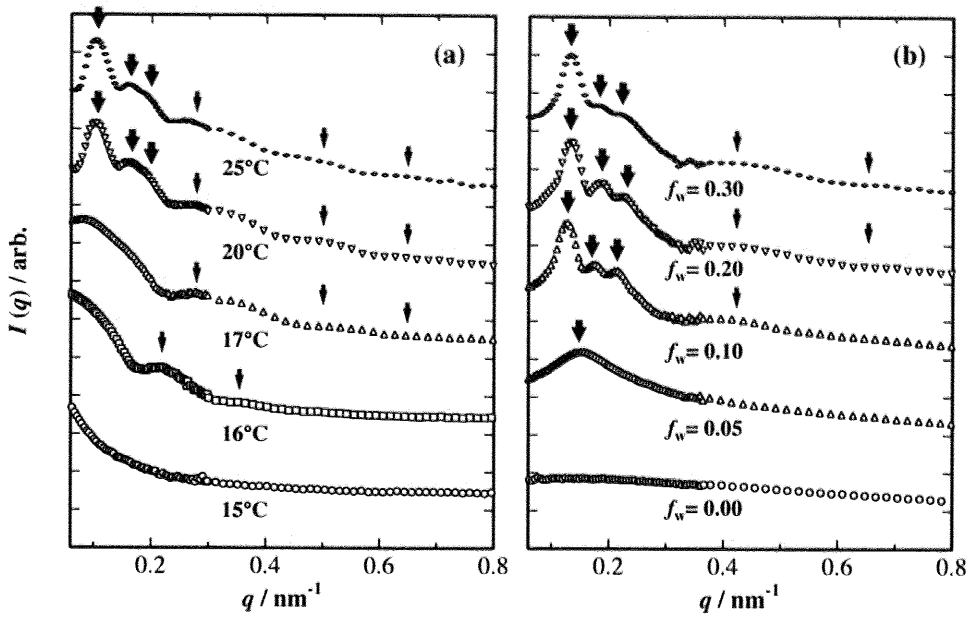


Figure 5.12: Variations of $I(q)$s for (a) 20 wt% EOVE-*b*-MOVE aqueous solution (heat-induced microphase-separated structure) with $T$ and (b) 12 wt% PhOVE-*b*-MOVE/acetone/water solution (water-induced microphase-separated structure) with the fraction of water added to the solution, $f_w$.

solution with increasing $T$ and (b) 12 wt% PhOVE-*b*-MOVE/acetone/water varying $f_w$. The thin and thick allows indicate the scattering peaks from the spherical domains and from the ordering of the domains, respectively. As shown in the figure, these two solutions show different responses to the external stimuli, i.e., (a) temperature increase (heat-induced transition) and (b) water addition (solvent-induced transition). The EOVE-*b*-MOVE system first forms micelles (indicated with the thick arrows) followed by packing of the micelles on increasing temperature (thin arrows). On the other hand, the PhOVE-*b*-MOVE keeps spatial ordering irrespective of $f_w$ (thick arrows) before polyPhOVE domain formation (thin arrows). These differences may be ascribed to the differences in the nature of molecular interactions associated in the microphase separation, i.e., hydrophobic interaction (heat-induced transition) and van der Waals interaction (solvent-induced transition). In the case of the former, the interaction parameter, $\chi$, changes step-wise change near the transition temperature. Poly(*N*-isopropyl acrylamide) in water is a typical system, in which $\chi$, changes discretely as was reported by Hirotsu.[7] In this case, the lower critical solution temperature (LCST) of polyEOVE in water is about 20 °C. By approaching

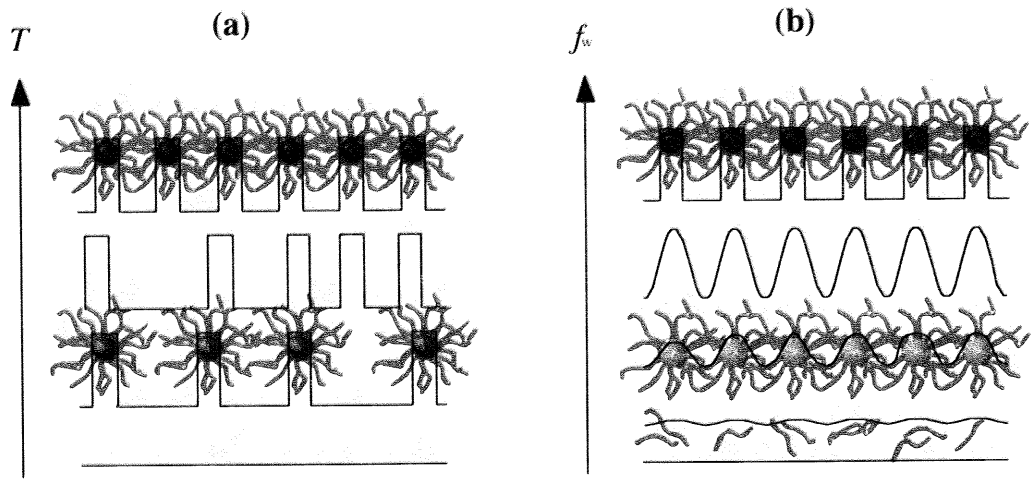


Figure 5.13: Schematic representations showing the difference in the growth of microphase-separated structure for (a) heat-induced and (b) water-induced phase separations.

this temperature, micelles (i.e., microdomains) consisting of polyEOVE chains are formed, which is followed by packing to a bcc by further increase in temperature. On the other hand, in the case of solvent-induced microphase separation, $\chi$ increases monotonously with $f_w$ resulting in amplification of the concentration fluctuations to form microphase separated structure.

Figure 5.13 illustrates the difference in the evolution processes of the structures by (a) heat-induced and (b) water-induced microphase separations. In the case of (a), micelles with polyEOVE chains are formed, followed by rearranging to a bcc packing as was reported in Chapter 3.[3] This results in a physical gelation. On the other hand, in the case of (b), an amplification of concentration fluctuations takes place due to an increase in $\chi$. Hence, the long spacing of the microdomain structure is fixed in advance to the formation of domains. This type of evolution process in concentration fluctuations is analogous to the spinodal decomposition. Further analyses along this aspect is in progress.

## 5.4 Conclusion

The microphase separated structure of the PhOVE-*b*-MOVE/acetone/water was investigated by SANS. The following facts were revealed: (1) By adding water, microphase separated structures consisting of spherical domains aligned in a bcc style

is formed. (2) The structure parameters are around $R = 13.0$ nm with $a = 79.0$ nm and $R = 14.0$ nm with $a = 65.0$ nm respectively for $C = 7$ and 12 wt%. (3) By the contrast changing experiment, it is confirmed that the spherical domains are constructed with polyPhOVE chains. (4) The mechanism of microphase separations is different between the heat-induced and water-induced microphase separations. The former is initiated by micelle formation followed by rearrangement to a bcc packing, and the latter is an amplification process similar to spinodal decomposition by keeping the long period correlation. Finally, it should be noted that these sharp environmental-sensitive microphase separation could be achieved with a tailor-made block copolymer carrying environment-sensitive functional groups, i.e., ether moiety in this case, in addition to a narrow molecular weight distribution.

# References


[1] Sugihara, S.; Matsuzono, S.; Sakai, H.; Abe, M.; Aoshima, S. *J. Polym. Sci. Part A: Polym. Chem.* 2001, **39**, 3190.

[2] Stanley, H. E. *Introduction to Phase Transition and Critical Phenomena*; Oxford University Press: New York, 1971.

[3] Okabe, S.; Sugihara, S.; Aoshima, S.; Shibayama, M. *Macrmolecules* 2002, **35**, 8139.

[4] Dingenouts, N.; Norhausen, C.; Ballauff, M. *Macromolecules* 1998, **31**, 8912.

[5] Hashimoto, T.; Shibayama, M.; Kawai, H. *Macromolecules* 1983, **16**, 1093.

[6] Shibayama, M.; Hashimoto, T.; Kawai, H. *Macromolecules* 1983, **16**, 16.

[7] Hirotsu, S. *J. Chem. Phys.* 1991, **94**, 3949.